

3D Printed Heat Exchangers

An Experimental Study

by

Gokul Chandrasekaran

A Thesis Presented in Partial Fulfillment
of the Requirements for the Degree
Master of Science

Approved April 2018 by the
Graduate Supervisory Committee:

Patrick Phelan, Chair
Konrad Rykaczewski
Karl Schultz

ARIZONA STATE UNIVERSITY

May 2018

ABSTRACT

As additive manufacturing grows as a cost-effective method of manufacturing, lighter, stronger and more efficient designs emerge. Heat exchangers are one of the most critical thermal devices in the thermal industry. Additive manufacturing brings us a design freedom no other manufacturing technology offers. Advancements in 3D printing lets us reimagine and optimize the performance of the heat exchangers with an incredible design flexibility previously unexplored due to manufacturing constraints.

In this research, the additive manufacturing technology and the heat exchanger design are explored to find a unique solution to improve the efficiency of heat exchangers. This includes creating a Triply Periodic Minimal Surface (TPMS) geometry, Schwarz-D in this case, using Mathematica with a flexibility to control the cell size of the models generated. This model is then encased in a closed cubical surface with manifolds for fluid inlets and outlets before 3D printed using the polymer nylon for thermal evaluation.

In the extent of this study, the heat exchanger developed is experimentally evaluated. The data obtained are used to derive a relationship between the heat transfer effectiveness and the Number of Transfer Units (NTU).The pressure loss across a fluid channel of the Schwarz D geometry is also studied.

The data presented in this study are part of initial experimental evaluation of 3D printed TPMS heat exchangers.Among heat exchangers with similar performance, the Schwarz D geometry is 32% smaller compared to a shell-and-tube heat exchanger.

ACKNOWLEDGMENTS

This study was accomplished under the mentorship of Prof Pat Phelan and with immense help from the Additive Manufacturing Group. I'm grateful to work under his mentorship. I also would like to thank my friends and family for supporting me throughout my Master's Program.

TABLE OF CONTENTS

	Page
LIST OF TABLES.....	v
LIST OF FIGURES	vi
NOMENCLATURE.....	viii
CHAPTER	
1 INTRODUCTION	1
1.1 Triply Periodic Minimal Surface.....	1
1.2 Additive Manufacturing.....	3
1.3 Heat Exchanger.....	5
2 APPROACH	7
2.1 Heat Exchanger Design.....	7
2.1.1 Fabrication.....	13
2.2 Experimental Setup.....	15
2.1.1 Data Acquisition.....	21
2.3 Errors and Uncertainties.....	23
2.4 Procedure for Analysis	24
3 RESULTS	25
3.1 Temperature	25
3.2 Heat Transfer Rate.....	30
3.3 ϵ V NTU Relationship	31
3.4 Pressure Drop	32
3.5 Comparison to Conventional Heat Exchangers	33

CHAPTER	Page
3.6 Estimating Overall Heat Transfer Coefficient, U	36
3.7 Discussions	37
4 CONCLUSION	38
5 FUTURE WORK	39
REFERENCES	40
APPENDIX	
A MATHEMATICA CODE.....	42
B STEADY STATE TEMPERATURE DATA	44

LIST OF TABLES

Table		Page
1.	Thermal Properties of Nylon -12 (PA 2200).....	15
2.	Summary of Uncertainties in the Experiment.....	26
3.	Average Steady State Temperature Data	25
4.	Different Heat Transfer Rates Calculated from the Data	30
5.	Pressure Measurements	32
6.	Friction Factors for Schwarz D Geometry and Shell-and-tube.....	35

LIST OF FIGURES

Figure	Page
1. Plateau's Memory by A.van der Net.....	1
2. Schwarz D, Schwarz G, Schwarz P geometries	2
3. A Representation of Schwarz D Geometry using Mathematica	3
4. EOS P110 SLS printer	5
5. Dynamic Window in Mathematica to Manipulate the Schwarz D Geometry	8
6. Discretized Graphic of the Schwarz D Geometry	9
7. Geometry Region Meshed	10
8. Heat Exchanger in STL Format Generated using Mathematica	11
9. Heat Exchanger with Defined Fluid Channels	12
10. X-Ray View of the Heat Exchanger.....	12
11. Visualizing the Two Flow Paths (Red and Blue) Inside a Schwarz D Core	13
12. Fabricated Schwarz D Heat Exchanger	14
13. Photograph of the Experimental Setup.....	16
14. Schematic of the Experimental Setup	16
15. Thermocouple Arrangement in Hot Fluid Side	17
16. Manometer Arrangement	18
17. Hot and Cold Fluid Reservoirs along with the Ice Chest on the Cold Side	19
18. Side View of the Heat Exchanger Mounted in the Setup	20
19. Top View of the Heat Exchanger Mounted in the Setup	21
20. Thermostat used for Calibrating the Thermocouples	22
21. Temperature Profile of Hot Inlet and Outlet Temperatures for Trial 2	27
22. Temperature Profile of Cold Inlet and Outlet Temperatures for Trial 2	28

Figure	Page
23. Transient State Response in Hot Side for Trial 2	29
24. Transient State Response in Cold Side for Trial 2.....	29
25. ϵ v NTU Data for Different Capacity Ratios	31
26. Pressure Loss v Flow Rate in Schwarz D Heat Exchanger	33
27. Friction Factor v Reynolds Number.....	36

NOMENCLATURE

T_{hi}	Hot Inlet Temperature [°C]
T_{ho}	Hot Outlet Temperature [°C]
T_{ci}	Cold Inlet Temperature [°C]
T_{co}	Cold Outlet Temperature [°C]
L_e	Entrance Length [m]
Re	Reynolds Number [-]
d	Pipe Diameter [m]
\dot{V}	Fluid Flow Rate [m ³ s ⁻¹]
\dot{Q}	Heat Transfer [W]
C_p	Specific Heat of Water [J kg ⁻¹ K ⁻¹]
ρ	Density of Water [kg m ⁻³]
δ	Incremental Change [-]
U	Overall Heat Transfer Coefficient [W m ⁻² K ⁻¹]
A	Area [m ²]
ΔT_{LM}	Log Mean Temperature Difference [°C]
ΔT_1	Temperature Difference at the Hot inlet [°C]
ΔT_2	Temperature Difference at the Hot outlet [°C]
NTU	Number of Transfer Units [-]
ε	Effectiveness Ratio [-]
C_r	Capacity Ratio [-]
ΔP	Pressure Difference [psi]

D_H	Hydraulic Diameter [m]
V_t	Total Volume [m ³]
V_m	Material Volume [m ³]
V_f	Fluid Volume [m ³]
L_{eff}	Effective Length [m]

CHAPTER 1

INTRODUCTION

1.1 Triply Periodic Minimal Surfaces (TPMS)

A minimal surface can be defined as a local-area-minimizing surface in a defined perimeter. Common examples of minimal surfaces are soap films in a bounded space which, due to surface tension, form a surface minimizing the local surface area. The minimal surface is a solution for Plateau's problem, defined as a part of calculus of variations by Lagrange in 1760[1]. If we extend the soap film definition of the minimal surface in a three-dimensional Euclidian space, we get a unique geometry for any given bounded space. These minimal surfaces, by definition, have a zero-mean curvature [2]. A common soap film example of a minimal surface is shown in Fig.1.

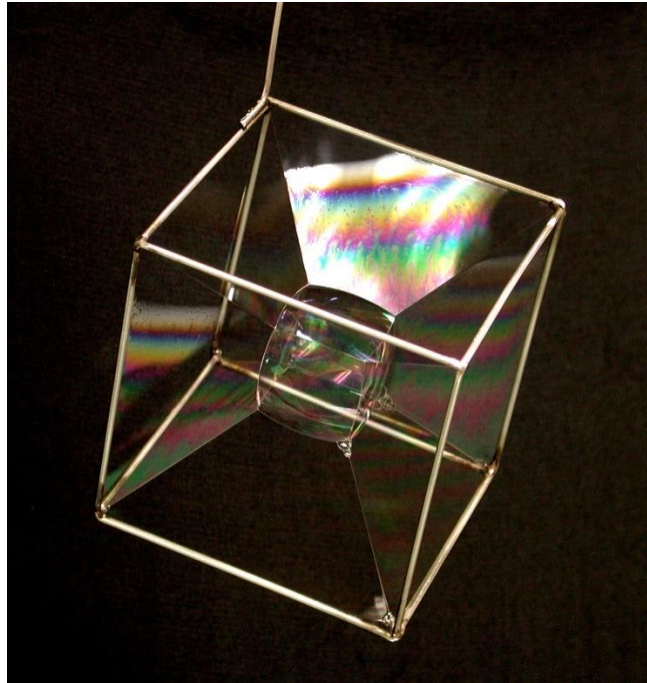


Fig 1: Plateau's Memory by A. van der Net [3]

Hermann Schwarz originally described periodic minimal surfaces in the 1880s with his student E.R. Neovius. After defining suitable polygons in a unit cell, they used the solution

for Plateau's problem for a polygon and symmetry arguments to construct the periodic surfaces. These were later named by Alan Schoen in his report [2] where he identified several new examples of periodic minimal surfaces.

For topological genus definitions, the Schwarz minimal surfaces fall under genus 3, meaning they fall under triply periodic minimal surfaces. In rough terms, genus 3 surfaces have 3 holes in the surface. Alan Schoen studied the partition of the three-dimensional Euclidian space into two interpenetrating labyrinths by intersection-free infinitely repeating periodic minimal surfaces [2]. Alan Schoen named these symmetric surfaces in three-dimensions based on the space group they resemble. They are commonly referred by the common names assigned by crystallographers to the lattices they represent, namely, P (primitive), G (gyroid), D (diamond), etc. as shown in Fig. 2[4].

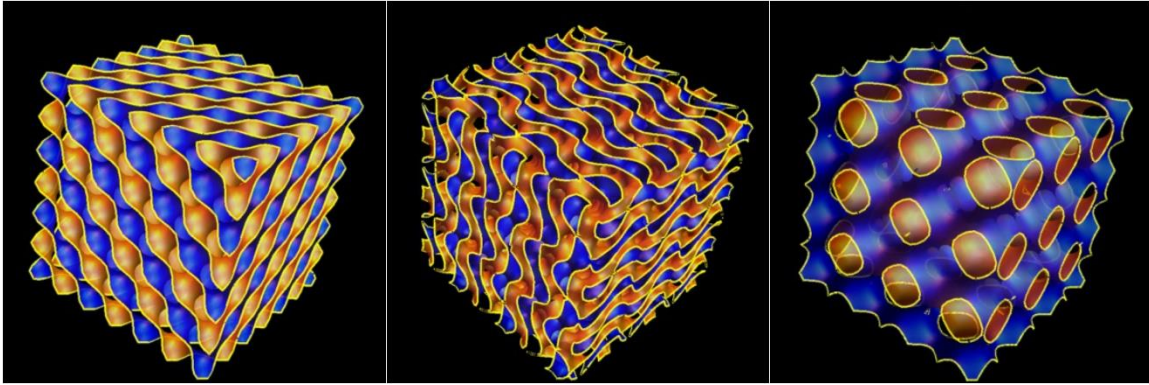


Fig 2: Schwarz D, Schwarz G, Schwarz P geometries.

The primary focus of this study is the Schwarz D (diamond). It resembles an inflated tubular version of the tetrahedral bond structure found between carbon atoms in a diamond, with two intertwined congruent labyrinths. A TPMS is balanced, if it has congruent labyrinths like Schwarz P and D. Schwarz derived a Weierstrass approximation with elliptic integrals to

define these surfaces [2]. But these integrals can be approximated to an implicit surface defined by the following expression [2]:

$$\begin{aligned} &\sin(x) \sin(y) \sin(z) + \sin(x) \cos(y) \cos(z) + \\ &\cos(x) \sin(y) \cos(z) + \cos(x) \cos(y) \sin(z) = 0 \end{aligned} \quad (1)$$

This expression is commonly used while modelling and prototyping the Schwarz D geometry. One type of Schwarz D geometry is shown in Fig. 3.

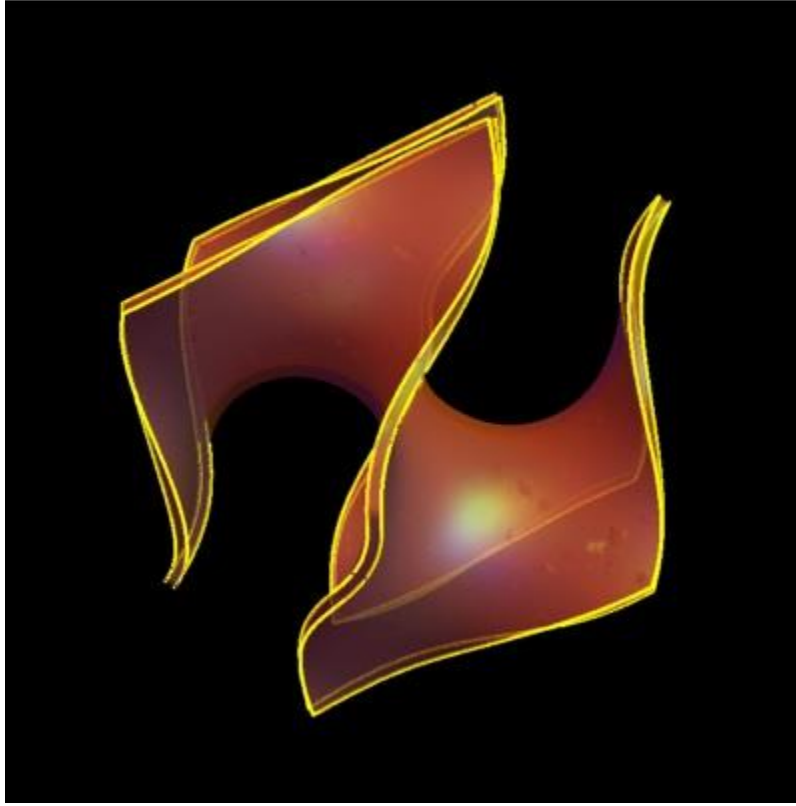


Fig. 3: A representation of a Schwarz D geometry using Mathematica.

1.2 Additive manufacturing

Additive manufacturing is a term describing any manufacturing process that builds a 3D object by adding material layer-by-layer. The manufacturing process includes using a computer and a 3D modelling software to model the object which is fed through to the equipment which builds each layer to construct a 3D object.

Additive manufacturing offers flexibility in prototyping that is fast, cheap and easy to manufacture. It offers a more efficient resource utilization in the manufacturing process by minimizing material waste compared to traditional methods of manufacturing [5]. More industries are considering additive manufacturing as a cost-effective method of manufacturing. We can rethink established designs and processes that were dictated by constraints due to manufacturing.

FDM is the most common additive manufacturing method and is based on a process that uses some form of thermoplastic polymer which turns into a liquid state and solidifies soon after its contact with the built layer. The most common desktop 3D printers use materials like PLA (Polylactic acid), ABS (Acrylonitrile Butadiene Styrene), HIPS (High Impact Polystyrene), etc. These materials are inexpensive and are used for prototyping to visualize a product. Desktop printers have a low-quality surface finish but are often great to test some prints before printing the parts on high-end printers. In this study, the prototype printed heat exchanger was built on an FDM printer using PLA.

High-end printers from manufacturers like EOS (Fig.4) use another method of additive manufacturing known as Selective Laser Sintering (SLS), more specifically a powder bed SLS. In this process a layer of powdered material is fused into the desired shape with high powered lasers. Unlike the FDM printers, the build is supported by the unsintered powder from the previous layers. The material used in this study is PA 2200 – Polyamide White or Nylon 12. It provides high detail resolution and has the highest quality of surface finish among the polymers discussed.



Fig 4: EOS P110 SLS printer. [3]

1.3 Heat exchanger

A heat exchanger is a thermal device used to transfer heat between two media, for example solid to fluid or between two or more fluids. In most fluid-to-fluid heat exchangers, the fluids are separated by a solid wall to prevent mixing. The shell-and-tube and plate-fin heat exchangers are the most commonly used types of heat exchangers due to their simplistic design and ease of manufacturing. This simplicity comes at the cost of weight and the material cost associated with it. In addition to that, the metals used in heat exchangers need special treatments to prevent corrosion from the working fluids further emphasizing the need for a better alternative.

Over the last decade, several studies on polymer heat exchangers were conducted to find a suitable combination of non-corrosive, light weight, cheaper and easily manufacturable material [7][8]. The polymers can significantly improve the life and performance of the heat

exchangers due to their antifouling and anticorrosive properties. Polymer heat exchangers are lighter weight than their metal counterparts and thus reduce the costs of the heat exchanger and the structural supports also become lighter [7].

Some of the studies in recent years have applied additive manufacturing technologies like 3D printing to design and fabricate heat exchangers [7][8][9]. The common heat exchangers found in these studies are again the familiar shell-tube and plate-fin type heat exchangers. The study by Martinus et al. [8], on air-water straight plate-fin polymer heat exchangers produced comparable results with a commercial product. This reinforces the need for innovations in heat exchanger materials.

Though introduction of additive manufacturing technology offers an immense design flexibility only a very few heat exchanger studies focus on designs other than shell-and-tube or plate-fin. One such study is based on microfluidic membrane devices and estimates the structure-dependent performance of microfluidic heat exchangers with sheet-like triply-periodic minimal-surface (TPMS) architectures [9]. The TPMS geometries, namely Schwarz P, D, G were fabricated and it was found that the Schwarz D geometry exhibited the best heat transfer characteristics with respect to inherent pressure drop [9]. It provides the motivation for this study which is aimed at evaluating the performance of a 3D-printed Schwarz D heat exchanger, but on a macro rather than a micro scale.

CHAPTER 2

APPROACH

The present study involves testing the performance of a heat exchanger that is drastically different from existing conventional designs. A heat exchanger is designed, built and fabricated to conform to the triply periodic minimal surface (TPMS), with defined inlets and outlets for the heat transfer fluids. A custom test rig is designed and built to obtain the necessary data for all the parameters needed to analyze the performance of the system. This section details several aspects of design considerations for both the heat exchanger and the experimental setup.

2.1 Heat exchanger design

The heat exchanger in this study is a triply periodic minimal surface with a diamond lattice structure known as Schwarz D. This geometry is defined by the implicit expression [2]:

$$\begin{aligned} \sin(x) \sin(y) \sin(z) + \sin(x) \cos(y) \cos(z) + \\ \cos(x) \sin(y) \cos(z) + \cos(x) \cos(y) \sin(z) = 0 \end{aligned} \quad (1)$$

We can use this equation to define the Schwarz D geometry in any mathematical plotter or Computer Aided Design (CAD) software. Initial attempts were made to visualizing the geometry, using MathMod ver. 5.1, of a 4-channel Schwarz D model. The software which was great for visualizing mathematical models was limited, however, when it came to the output file formats. The 3D printers commonly use a STL file format (abbreviated for stereolithography, a common additive manufacturing process) which gives the raw

unstructured triangulated surface and normal to define a 3D object. This enables cross platform compatibility among different types of 3D printers.

Generating these surfaces using raw data points in CAD software like SolidWorks and Autodesk Fusion proved a bit challenging. Wolfram Mathematica, however, offers a direct STL format geometry output from a 3D mesh plot. Using the documentation provided on TPMS on the Wolfram Demonstrations Project [4], several modifications were made to generate custom Schwarz D geometries in a single unit space as shown in Fig. 5 by moving the range bar from single unit cell to any desired number of flowchannels. The visual style and opacity of the geometry can be controlled by clicking on the respective buttons in the dynamic evaluation window as well as the number of recursions.

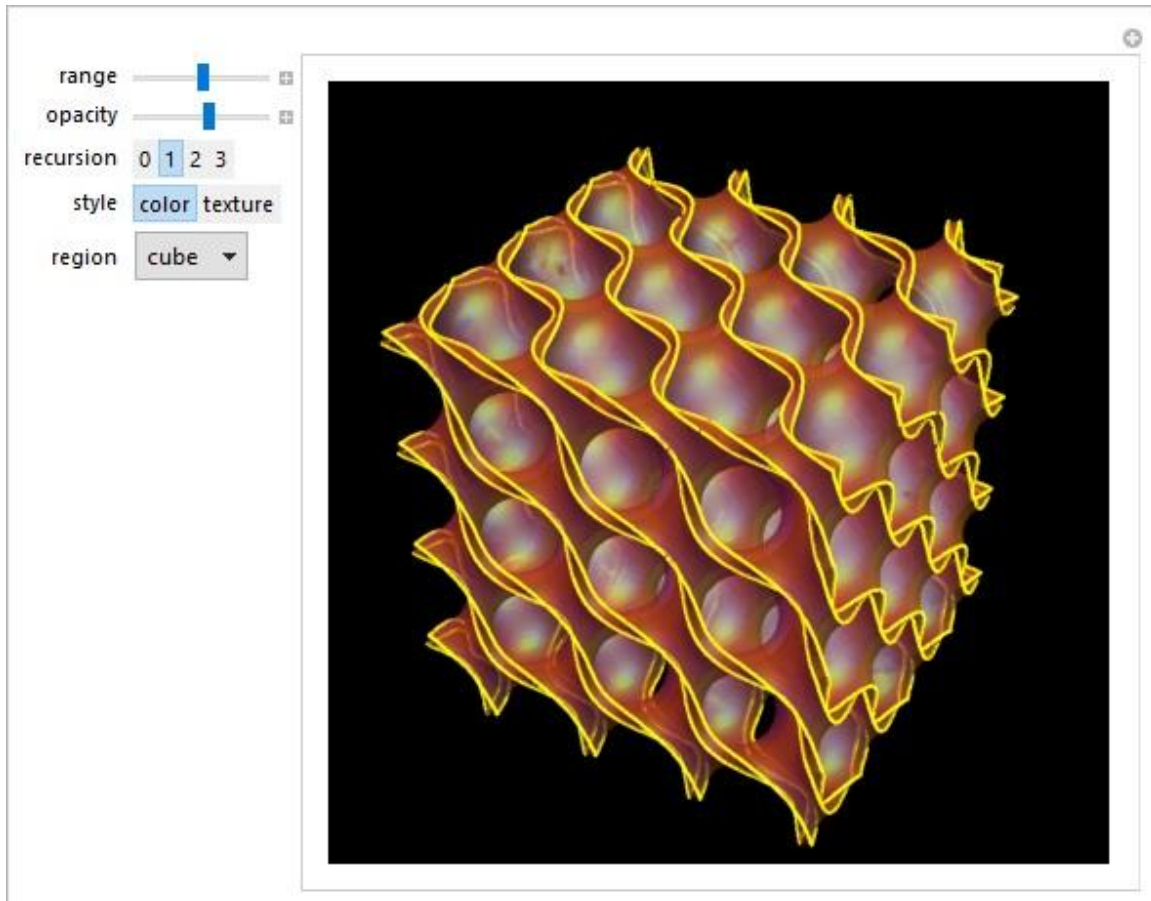


Fig 5: Dynamic window in Mathematica to manipulate the Schwarz D geometry.

The geometry is discretized using the “DiscretizeGraphics” command as shown in Fig.6, which is then meshed to get the final geometry.

```
In[2]:= geometry2 = DiscretizeGraphics[geometry]
```

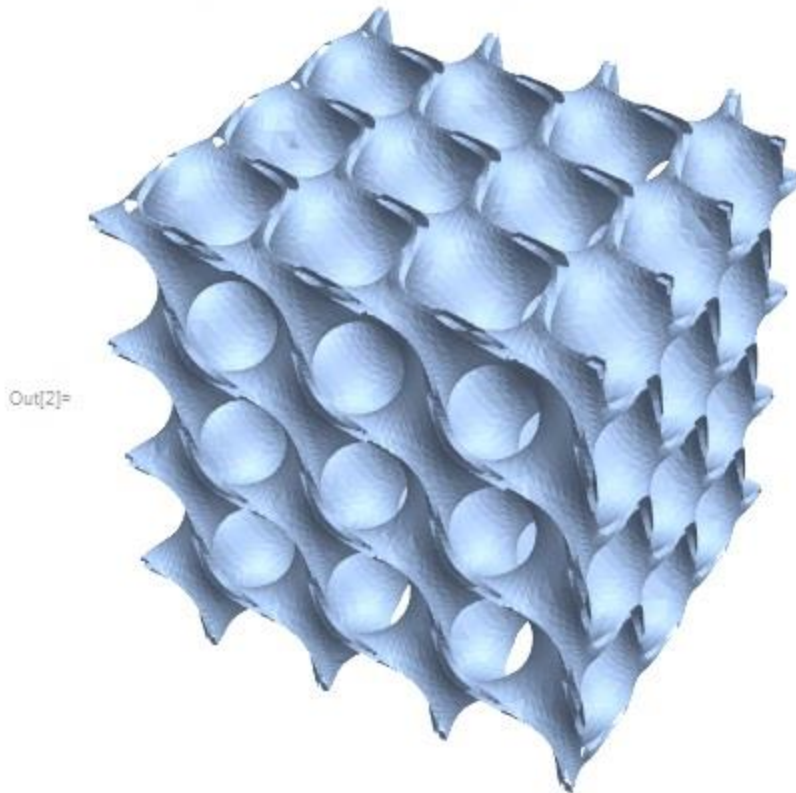


Fig 6: Discretized graphic of the Schwarz D geometry.

The final mesh geometry can be exported as an STL file format mesh that can be read directly by a 3D printer to produce a physical geometry as shown in Fig. 7. The output file is exported to the default document location and is saved as a file named “S_D1.stl”. The STL file can be accessed using built-in windows 3D Builder or any compatible CAD software.

```
In[3]:= geometry3 = MeshRegion[geometry2, PlotTheme -> "Lines"]  
Export["S_D1.stl", geometry3]
```

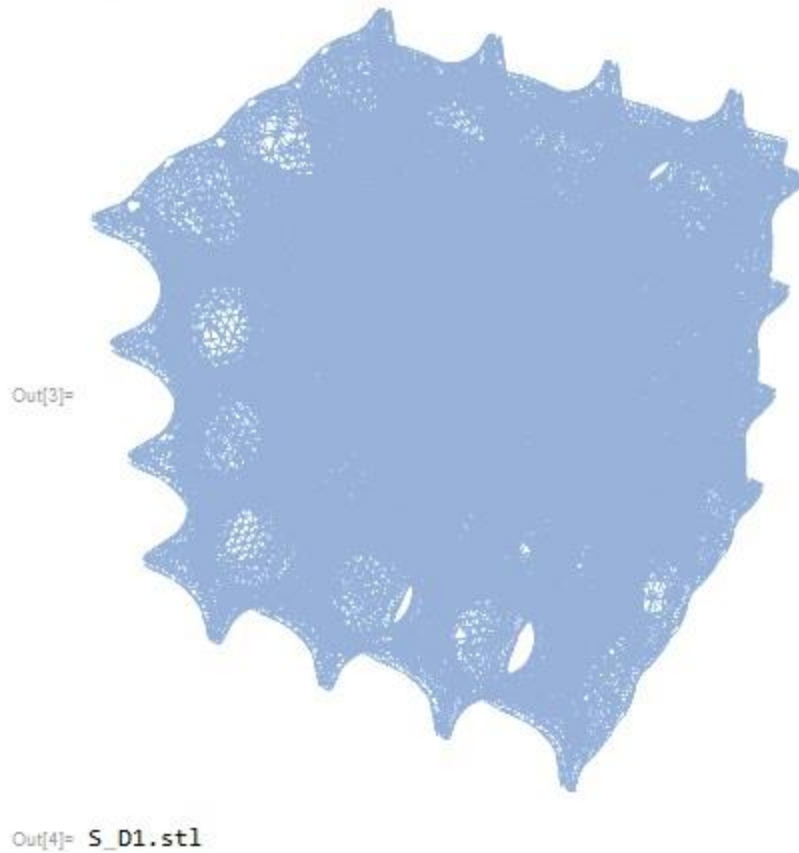


Fig 7: Geometry region meshed.

The geometry generated from Mathematica is an open heat exchanger without any defined boundaries or walls or any defined inlet and outlet as seen in Fig 8. The raw format of the STL files works to our advantage as it just defines the surfaces and not the scale of the 3D geometry. A single file can be used to print geometries of different sizes just by updating the dimension and scale used in that iteration. To simplify the manifolds, we can scale the geometry to match the outer diameter of the inlet and outlet pipes for a simple geometrical fit, in this case, 0.5in (12.7mm). This defines the scale of our heat exchanger, the inlets and the outlets.

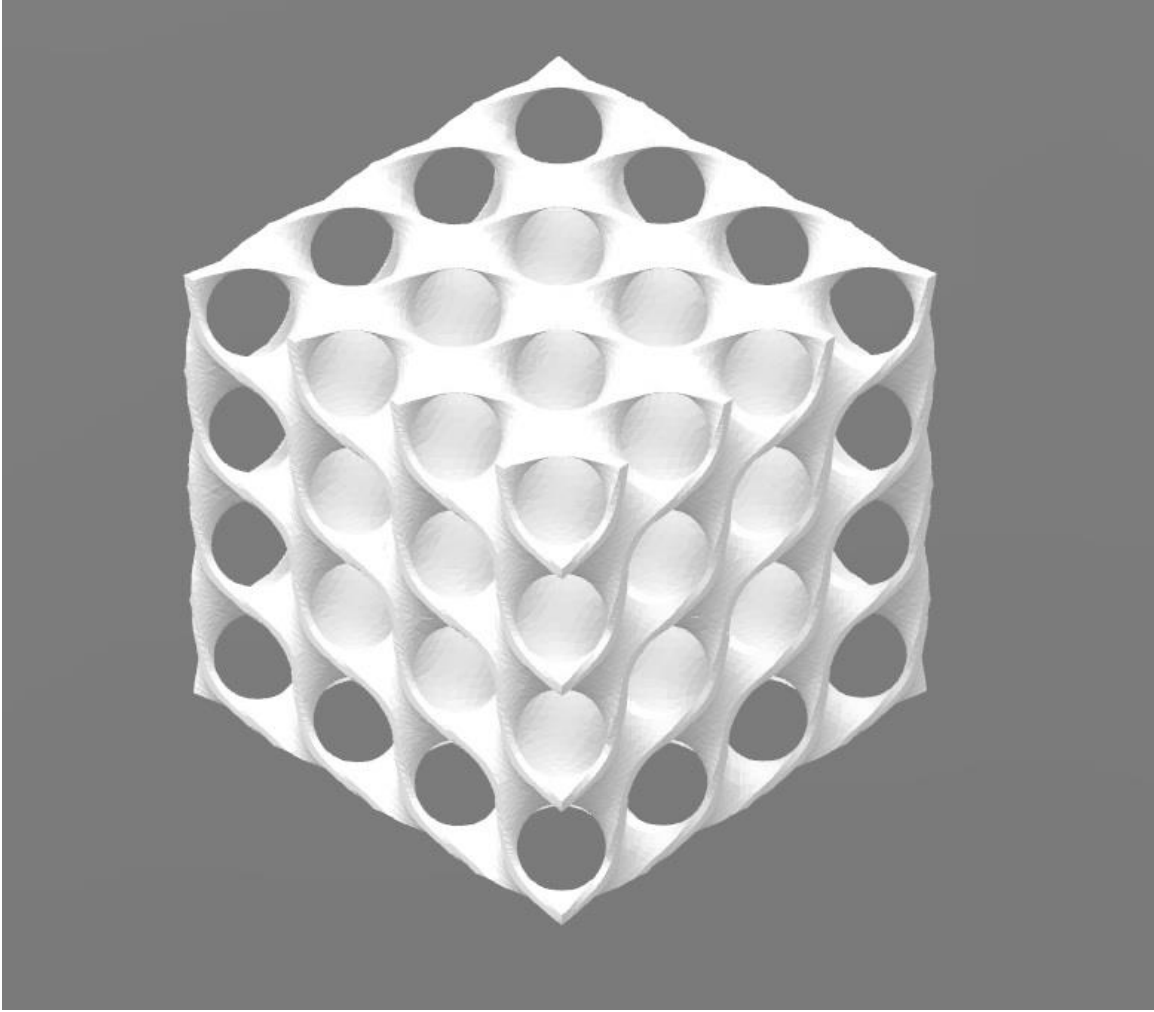


Fig 8: Heat exchanger in STL format generated using Mathematica.

After determining the scale of the heat exchanger, a boundary wall with defined openings for inlets and outlets can be modelled using SolidWorks. A boundary box with defined fluid lines is positioned over the heat exchanger with proper orientation. An incredible advantage with these TPMS surfaces is that every alternate channel is connected, so there are several points where we can define our inlets and outlets. The walls of the box are defined such that there is a solid enclosure between adjacent channels. The finished heat exchanger after encasing the boundary box and is shown in Fig. 9. The boundary box is a cube of side 10.8

cm (4.25 in) with a thickness of 0.3 cm (0.12 in). Figure 10 shows an X-ray view of the Schwarz geometry inside the boundary box.

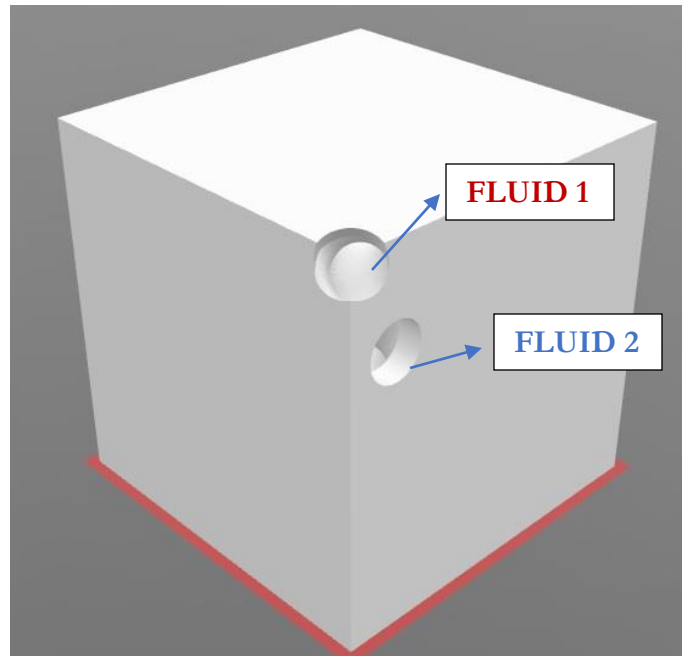


Fig 9: Heat exchanger with defined fluid channels.

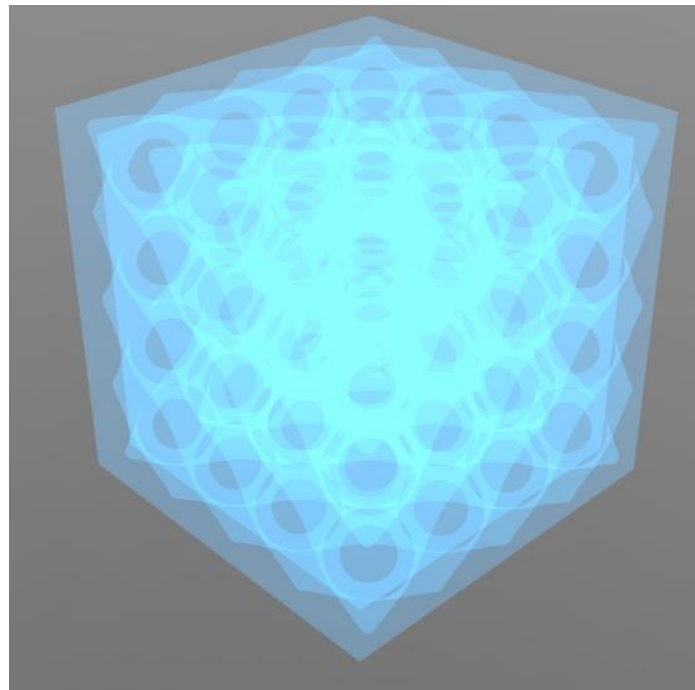


Fig 10: X-Ray view of the heat exchanger.

The flow paths inside the Schwarz D core can be visualized by creating a negative of the geometry in Fig 8. The flow paths in a Schwarz D core are shown in Fig. 11.

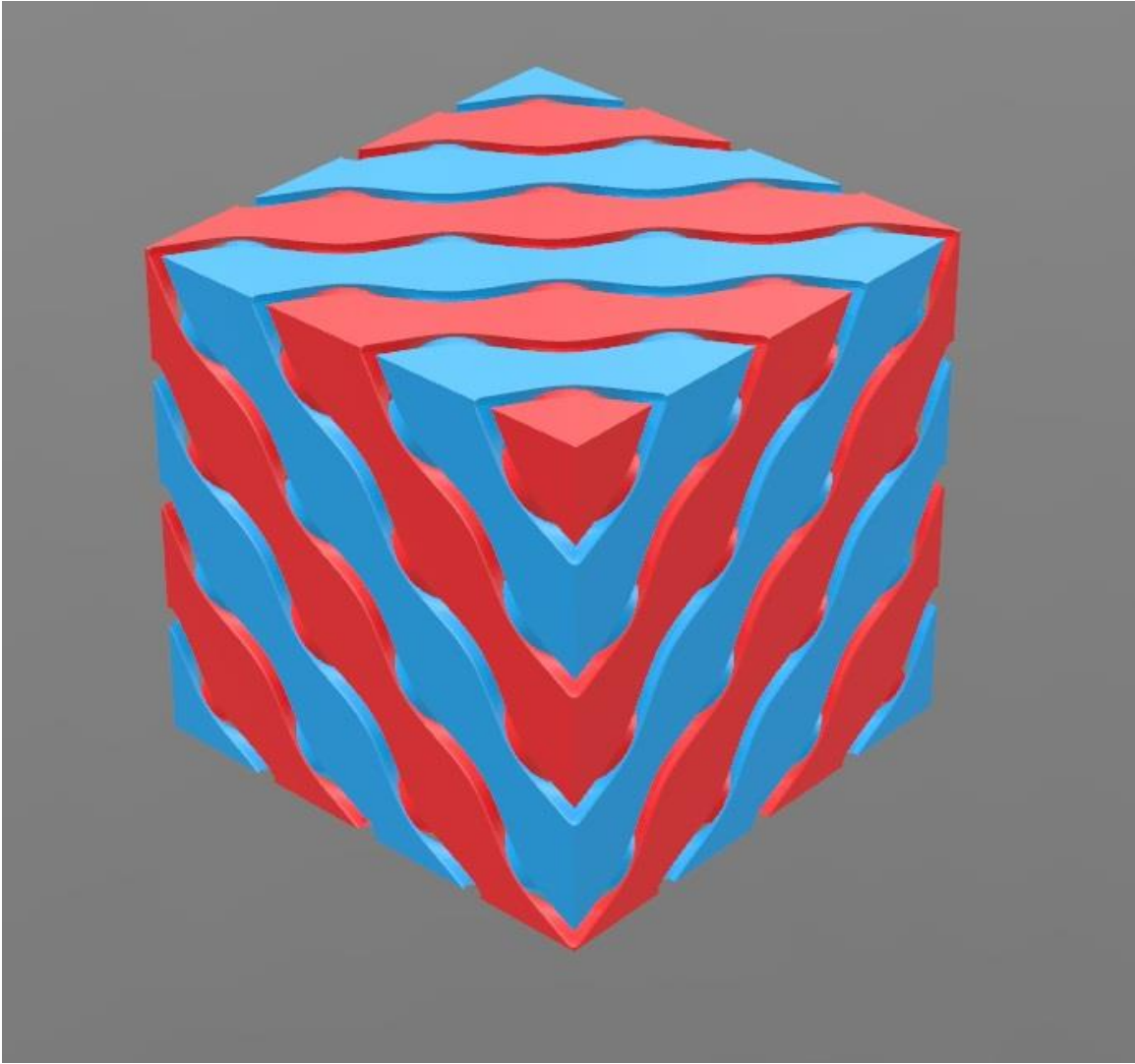


Fig 11: Visualizing the two flow paths (red and blue) inside a Schwarz D core.

2.1.1 Fabrication

After designing the heat exchanger, we must choose a method of fabrication. As discussed earlier, we have a variety of combinations of materials and printers we can use to print our model. Earlier attempts to print the model using PLA extruders like MakerBot replicator showed poor surface finish and dimensional tolerances. Finally, the model was printed using

PA-2200 or Polyamide, nylon 12 using an EOS P110 SLS printer by selectively sintering layer-by-layer using a high-powered laser on a powder bed.

We focus on finding a non-dimensional parameter to quantify heat transfer effectiveness and pressure loss for the given geometry. As a significant number of studies [7][8] have been conducted on polymer heat exchangers the present study provides additional data to characterize the performance of nylon-12. The fabricated model is shown in Fig. 12.

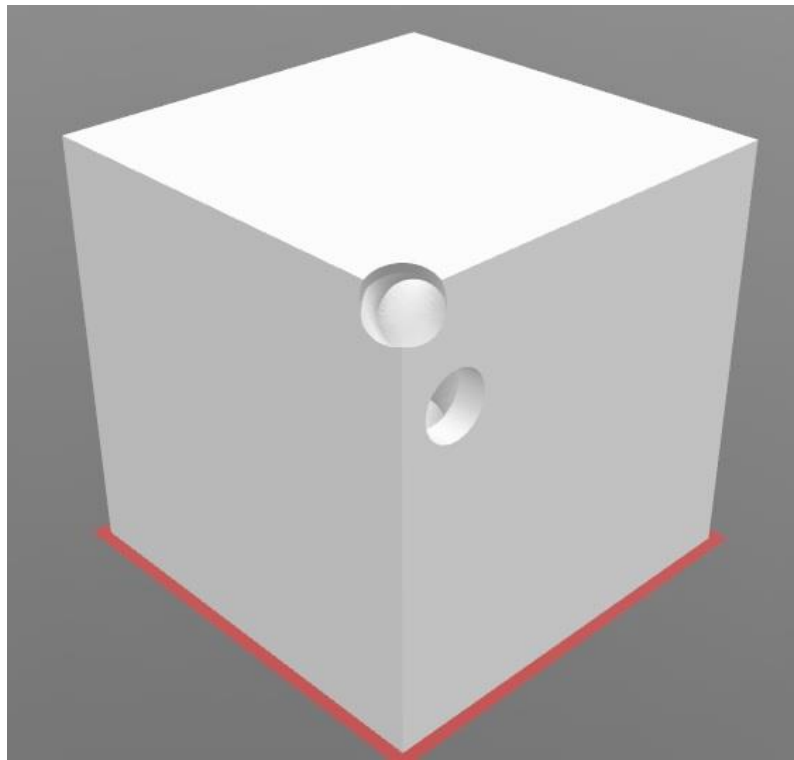


Fig 12: Fabricated Schwarz D heat exchanger

The thermal properties of Nylon-12 or PA 2200 can be found in Table 1.

Table 1: Thermal properties of Nylon-12 (PA 2200)[10]:

Property	Measurement Method	Value(units)
Thermal conductivity – Vertical to sintered layers	DIN52616	0.144 W m ⁻¹ K ⁻¹
~Thermal conductivity – Horizontal to sintered layers		0.127 W m ⁻¹ K ⁻¹
Water Absorption – 100°C saturation	ISO62/DIN53495	1.93%
Water Absorption – 23°C 96% RF		1.33%
Water Absorption – 23°C 50% RF		0.52%

2.2 Experimental setup

The experimental setup is designed to extract data to analyze the performance of the heat exchanger. The output of the experiments included 4 temperature measurements, T_{HI} , T_{CI} , T_{HO} , T_{CO} , flow rates on the hot and cold side, and the differential pressure across the hot side of the heat exchanger. Figure 13 shows a photograph of the experimental setup and Fig. 14 shows a schematic diagram for better understanding.

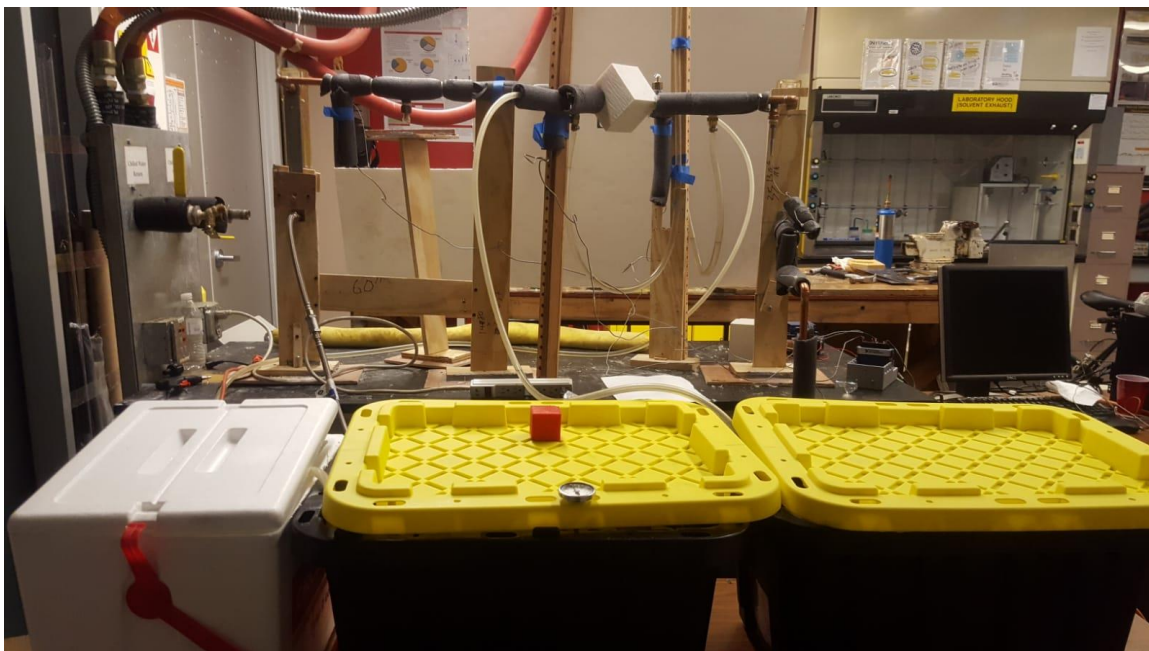


Fig 13: Photograph of the experimental setup

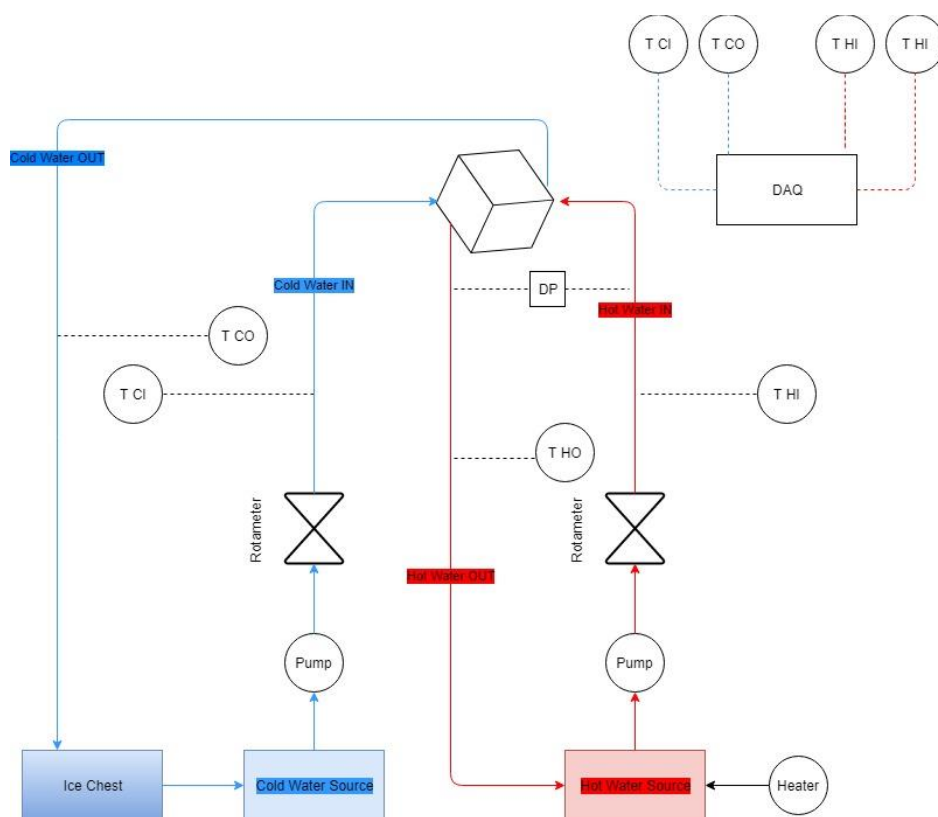


Fig 14: Schematic of the experimental setup.

The flow must be fully developed before it enters the heat exchanger. The volume flow rates in the experiment were regulated between 0.8 and 1.6 gpm (5.05 to $10.10 \times 10^{-5} \text{ m}^3 \text{ s}^{-1}$). The flow is turbulent, $Re > 4000$. So the entrance length is calculated using the equation [12]:

$$L_e = 4.4 R_e^{\frac{1}{6}} d \quad (2)$$

where L_e is the entrance length, R_e the Reynolds number, and d the diameter of the inlet pipe. For the maximum flow rate of 1.6 gpm ($10.10 \times 10^{-5} \text{ m}^3 \text{ s}^{-1}$), $L_e = 26.5 \text{ cm}$.

The temperatures for both the hot and cold channels are measured at the fluid inlet and outlet. Each temperature is measured using a calibrated Omega T-type beaded thermocouple with a 0.508 mm (0.20 in) diameter. The thermocouples are attached to the fluid line as shown in Fig. 15.

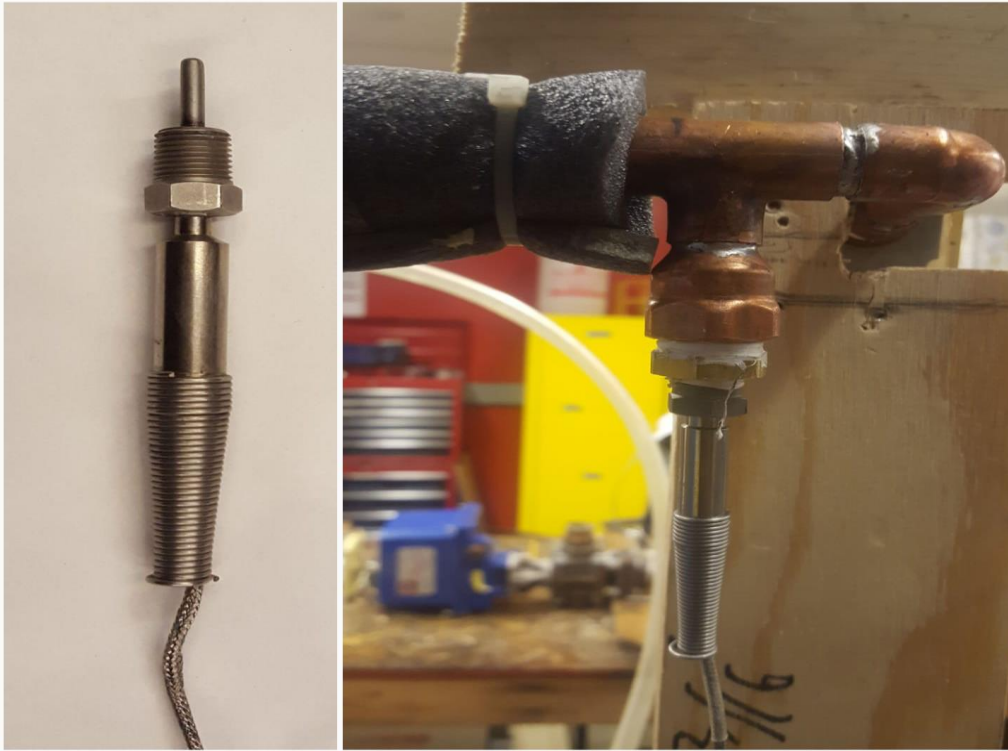


Fig 15: Thermocouple arrangement in the hot fluid side.

The initial pressure measurements were made using a Setra Model 230 True wet-to-wet Differential Pressure Transducer. But after the initial experiments it was found that the range of pressures observed was below the resolution of the transducer. A simpler alternative was to set up a U-tube manometer to measure the differential pressure. Two U-tubes were therefore configured, one on the inlet and outlet of the hot side and attached along a vertical scale. This gives us two water level measurements, one for each of the higher and lower pressure regions in the flow. The pressure difference across the hot side flow at different flow rates was measured as the difference in the water levels of the two manometers before converting the values into equivalent pressure by using $\Delta P = \rho \cdot g \cdot \Delta h$. The setup of the manometer is shown in Fig. 16.

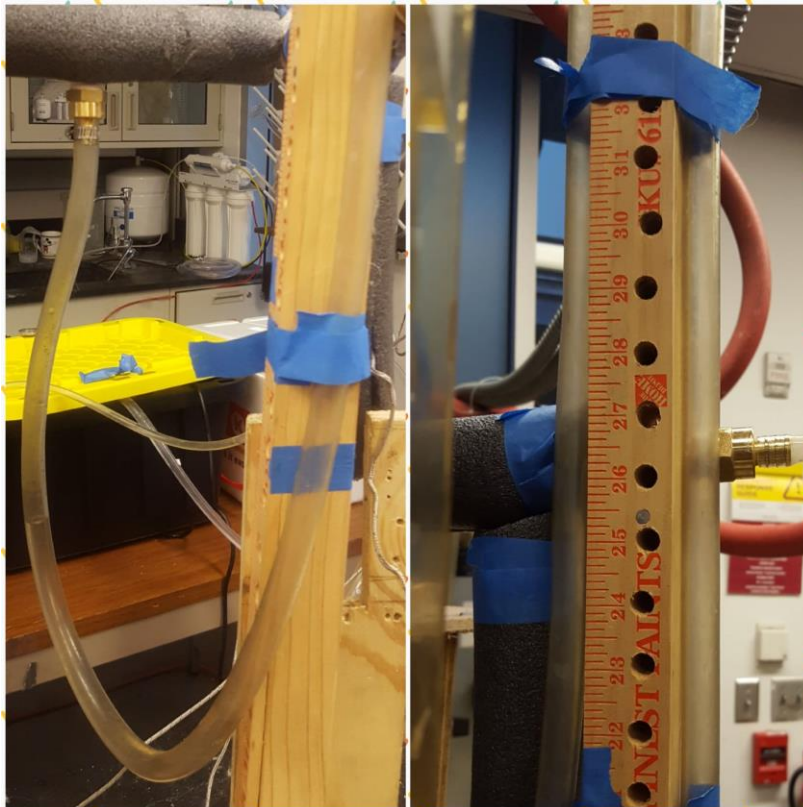


Fig 16: Manometer arrangement.

The flow was controlled by the valves attached to the rotameters positioned on both the hot and cold sides. The rotameters were calibrated by using the time taken to fill a graduated 3500 ml cylinder at a fixed flow rate.

The hot and cold side flows were controlled by using two pumps (EcoPlus 528 and EcoPlus 1000), where the cold side was controlled to a constant 0.8 gallon per minute (gpm) ($5.05 \times 10^{-5} \text{ m}^3 \text{ s}^{-1}$) flow rate and the hot side flow rate was regulated between 0.8 and 1.6 gpm (5.05 to $10.10 \times 10^{-5} \text{ m}^3 \text{ s}^{-1}$) for this experiment using the knobs on the rotameter. The hot side was heated with an immersion heater inside the reservoir. Initial trials suggested that the temperature difference in the hot side was small enough to recirculate the water. For the cold side, the flow was sent through an ice chest, filled with ice, before returning for recirculation. Figure 17 shows the fluid reservoirs with marked inlets and outlets.

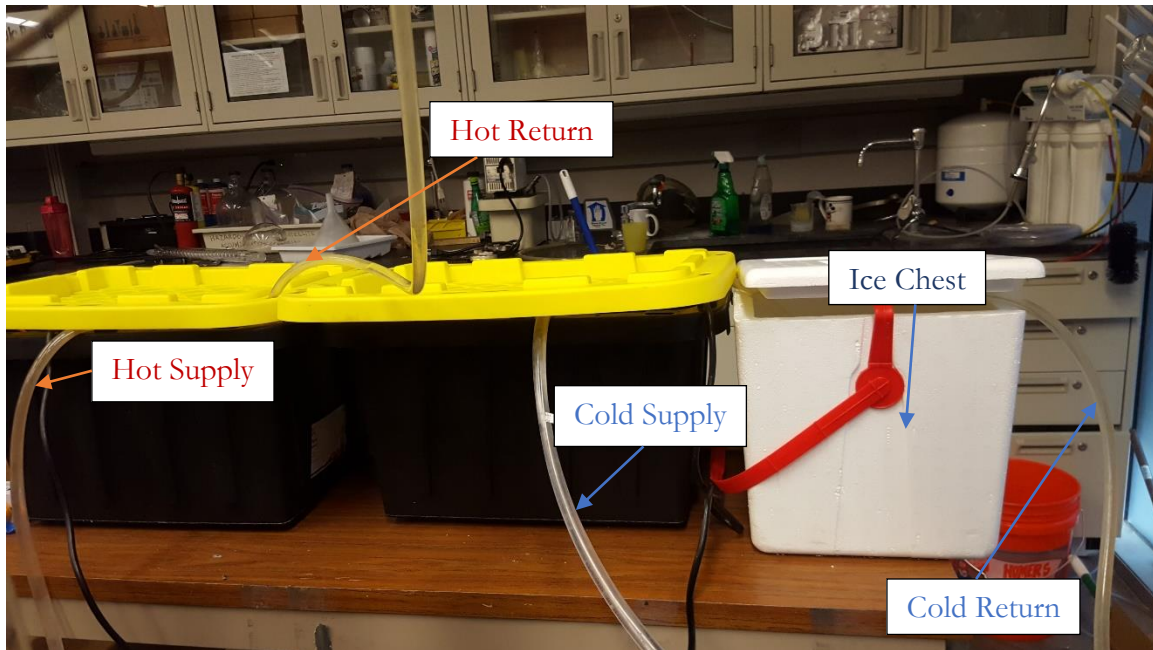


Fig 17: Hot and cold fluid reservoirs along with the ice chest on the cold side.

The setup was built using 0.5 in (12.7 cm) copper tubing and connectors to make it uniform. The tubes were connected using T-joints at the points where the temperature and pressure measurements were needed. All the joints were soldered to avoid any leaks as shown in Fig. 15, with all the ends soldered.

The heat exchanger which structurally fits in to the setup is sealed using hot glue, a common adhesive used with nylon-12 parts. Prior to data acquisition, all the exposed copper tubing was insulated using 0.25 in (6.35 mm) foam to avoid external heat input or heat losses. Figures 18 and 19 show the side view and the top view of the heat exchanger fixed completely into the setup. The cold side inlet and outlet is marked to provide a reference on how the heat exchanger is mounted.

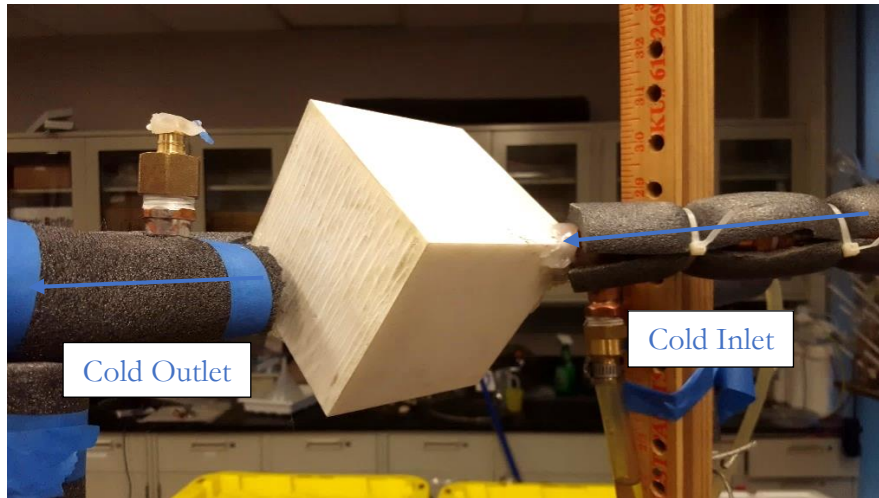


Fig 18: Side view of the heat exchanger mounted in the setup.

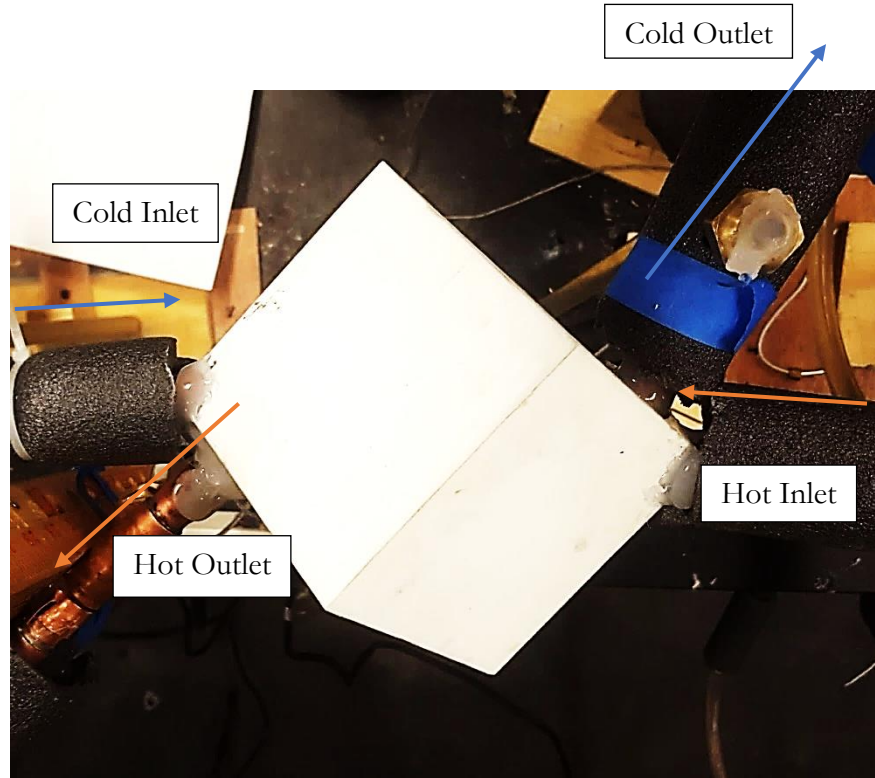


Fig. 19: Top view of the heat exchanger mounted in the setup.

2.2.1 Data acquisition

The flow rate and pressure data for this experiment are measured manually by reading the indicators in the instruments. Most of the temperature measurements, except for the reservoir temperatures, are collected using a National Instruments (NI) NI-9213 C series temperature input module mounted on a compact Data Acquisition (cDAQ) 9174 chassis.

We did not expect rapid temperature changes in the system, so the sampling rate was set at 1 S/s (samples/second). The thermocouples used were Omega T type beaded type thermocouples with a 0.508 mm (0.20 in) diameter. We already established how the thermocouples were mounted to the fluid channel in the previous section. The thermocouples were calibrated using a Thermo Scientific Haake DC10 P5 model thermostat,

shown in Fig. 20, which followed the thermostat reading to the nearest 0.05 °C. Each trial of the experiment was run till the temperature fluctuations in the data were within this limit.



Fig 20: Thermostat used for calibrating the thermocouples.

As discussed before the flow rates were measured using rotameters. A 3500-ml graduated cylinder was filled and timed using a stopwatch at different flow rates fixed on the rotameter. The data obtained from these measurements were close to the rotameter reading within ± 0.04 gallon/min.

During the calibration experiments conducted for the originally intended differential pressure transducers, the water column was connected to the high-pressure end and the low-pressure end was exposed to atmospheric pressure. The data collected between 10 inches and 43 inches of water column had less than 1% deviation from the actual pressure reading and followed a linear plot. The pressure difference in this experiment, however, after the initial trials was less than what could be easily resolved by the transducer.

Hence, for pressure measurements we had to resort back to the U-tube manometers. The pressure was measured by reading the length of the water column on the two manometers on the high and low-pressure side on the hot side of the heat exchanger and noting the difference in the height of the water column. This was compared to the standard inches of water to psi chart to get the pressure difference. In the worst-case scenario, our error in pressure measurement was between $\pm 8\%$, if the readings were misread.

2.3 Errors and uncertainties

As discussed in the previous section, our measurements have certain errors compared to the actual value. We can use the concepts from R.J Moffat's work on Uncertainty Analysis to determine the uncertainties in this experiment [12]. From the data obtained in this experiment, we can find the heat transferred, \dot{Q} , in the cold channel, for example, by using the following formula:

$$\dot{Q} = \dot{V} \cdot \rho \cdot C_p \cdot (T_{co} - T_{ci}) \quad (3)$$

where \dot{V} is the flow rate of the water, C_p the specific heat of water, T_{ci} the temperature of the water at the cold inlet, T_{co} the temperature of the water at the cold outlet and ρ the density of water. The cold side temperatures are low and are susceptible to a relatively large relative error, hence they are used to find the maximum uncertainty in measuring the heat transferred.

The steady-state relative error for the above expression can be found using:

$$\frac{\delta \dot{Q}}{\dot{Q}} = \left\{ \left(\frac{\delta \dot{V}}{\dot{V}} \right)^2 + \left(\frac{\delta T_{co}}{T_{co}} \right)^2 + \left(\frac{\delta T_{ci}}{T_{ci}} \right)^2 \right\}^{\frac{1}{2}} \quad (4)$$

Plugging in the average steady-state temperatures and flow rates for a given trial yields:

$$\frac{\delta \dot{Q}}{\dot{Q}} = \left\{ \left(\frac{0.04}{0.8} \right)^2 + \left(\frac{0.5}{6.21} \right)^2 + \left(\frac{0.5}{3.18} \right)^2 \right\}^{\frac{1}{2}} \quad (5)$$

In other words, the heat transfer rate, \dot{Q} , has a relative error of 18.36% for $\dot{Q} = 640.09$ W at the worst-case scenario for the heat transfer. The trial given here has the maximum relative error for the flow rate and the temperatures. Hence, it has the maximum relative error among all the trials studied.

The summary of all uncertainties expected in the experiment is shown in Table 2.

Table 2: Summary of uncertainties in the experiment:

Parameter	Uncertainty in measurement
Flow rate, \dot{V}	± 0.04 gpm
Temperature, T (thermocouple)	± 0.05 °C
Temperature, T (thermometer)	± 0.5 °C
Manometer, h	± 0.125 in

2.4 Procedure for analysis

We have the temperature values from all the trials. From this we derive \dot{Q} , the heat transfer rate on the hot side and the cold side.

We know that the Log Mean Temperature Difference (LMTD) method is used commonly for counter flow heat exchangers. We can relate \dot{Q} to the LMTD as follows [10]:

$$\dot{Q} = UA \Delta T_{LM} \quad (6)$$

where U is the overall heat transfer coefficient, A the heat transfer area, and ΔT_{LM} the Log Mean Temperature Difference defined by:

$$\Delta T_{LM} = \frac{\Delta T_1 - \Delta T_2}{\ln(\Delta T_1 / \Delta T_2)} \quad (7)$$

where for this counter-flow heat exchanger,

$$\Delta T_1 = T_{hi} - T_{co} \quad (8)$$

$$\Delta T_2 = T_{ho} - T_{ci} \quad (9)$$

We can invert Eq. 5 to determine UA as:

$$UA = \frac{\dot{Q}}{\Delta T_{LM}} \quad (10)$$

The NTU or Number of Transfer Units is a non-dimensional method to characterize a heat exchanger. NTU is defined by:

$$NTU = \frac{UA}{(\dot{m}C_p)_{min}} \quad (10)$$

Another parameter characterizing the heat exchanger is the heat exchanger effectiveness, ϵ , which is the ratio of the rate of heat transfer \dot{Q} , to the maximum theoretical heat transfer, \dot{Q}_{max} [10]:

$$\epsilon = \frac{\dot{Q}}{\dot{Q}_{max}} \quad (11)$$

$$\dot{Q}_{max} = (\dot{V} \cdot \rho \cdot C_p)_{min} \cdot (T_{hi} - T_{ci}). \quad (12)$$

We can use the data obtained to find a relationship between the effectiveness and the NTU.

CHAPTER 3

RESULTS

The data presented in this section are obtained under steady-state conditions. Steady state refers to the state where the inlet temperatures of both the hot and cold side vary less than $\pm 0.5^{\circ}\text{C}$ from their respective reservoirs. At the same time the data from the thermocouples are constant within a bandwidth of $\pm 0.05^{\circ}\text{C}$ for at least 30 seconds. It was observed that steady state was achieved within ~ 25 minutes of the start of the experiment. After each trial, the pumps were shut off and the system was allowed to cool off for 10 minutes before the next trial. After the trial began, the temperature data were monitored until the temperatures approached the reservoir temperature after which the data were logged until they reached steady state. At steady state an additional set of data was logged for further analysis.

3.1 Temperatures

Table 3: Average steady-state temperature data

Trial	$\dot{V} \text{ (hot)}$ (gpm)	T_{hi} ($^{\circ}\text{C}$)	T_{ci} ($^{\circ}\text{C}$)	T_{ho} ($^{\circ}\text{C}$)	T_{co} ($^{\circ}\text{C}$)	ΔT_1 ($^{\circ}\text{C}$)	ΔT_2 ($^{\circ}\text{C}$)	ΔT_{LM} ($^{\circ}\text{C}$)
1	0.8	32.58	8.15	32.23	8.36	24.22	24.08	24.15
2	0.8	44.77	17.81	44.28	18.33	26.44	26.47	26.45
3	1.2	40.16	5.39	39.82	8.61	31.55	34.43	32.97
4	1.2	30.54	3.18	30.16	6.21	24.34	26.98	25.64
5	1.2	33.07	3.58	32.66	6.52	26.55	29.08	27.80
6	1.6	39.94	7.68	39.70	8.50	31.44	32.02	31.73
7	1.6	30.83	6.55	30.66	7.34	23.49	24.11	23.80

Table 3 shows the average temperatures and mass flow rate for all the trials.

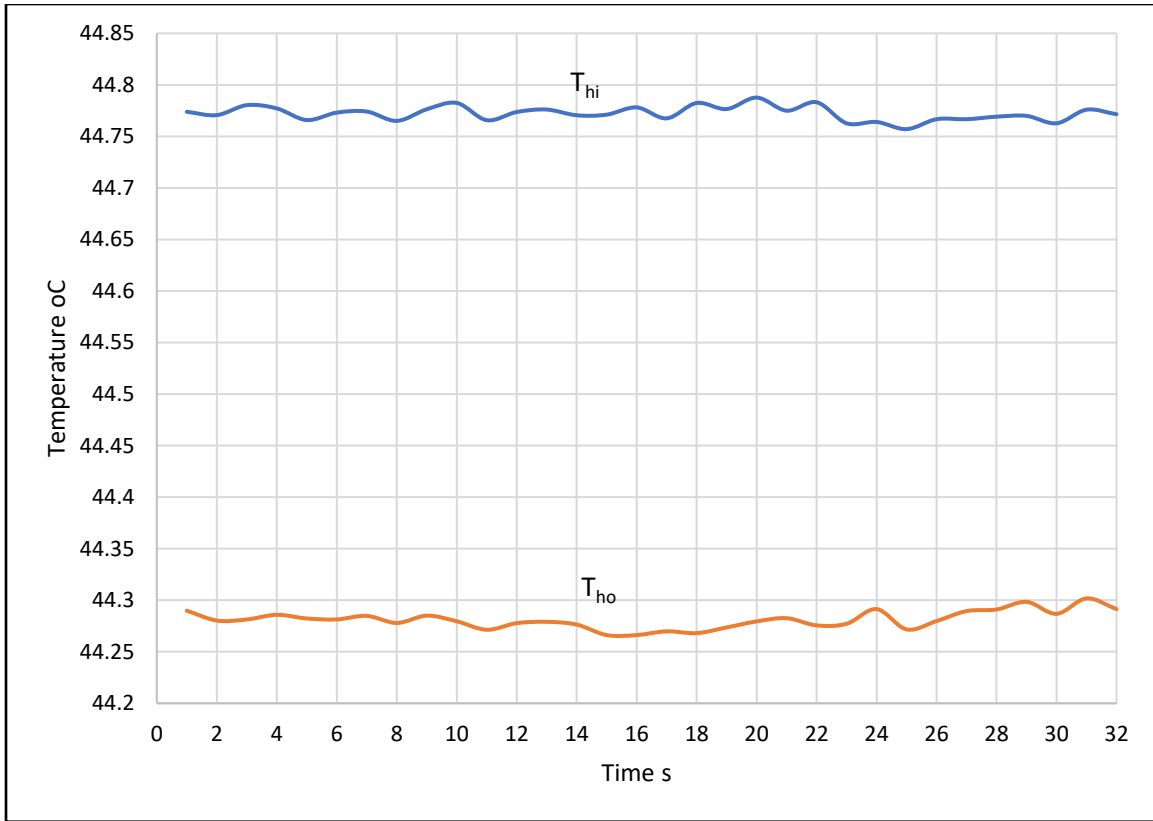


Fig 21: Temperature profile of the hot inlet and outlet temperatures for trial 2.

Figures 21 and 22 show the steady-state temperatures for trial 2 at the hot and cold channels. It can be observed that most points in the graphs are within the limits set for steady-state inlet and outlet temperatures.

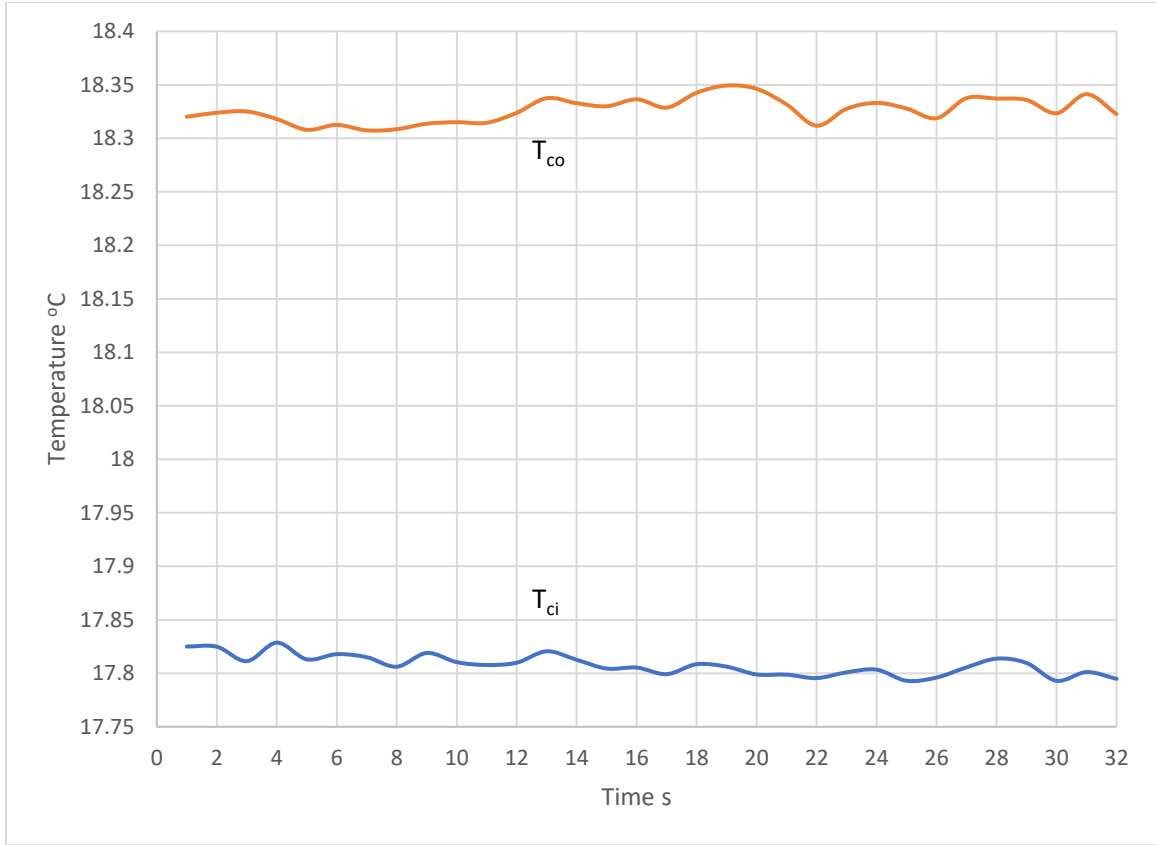


Fig 22: Temperature profile of the cold inlet and outlet temperatures for trial 2.

Figures 23 and 24 show the complete steady state plot for trial 2. The variance of last 40 data points in the plots are on the order of 10^{-4} , which was considered steadystate.

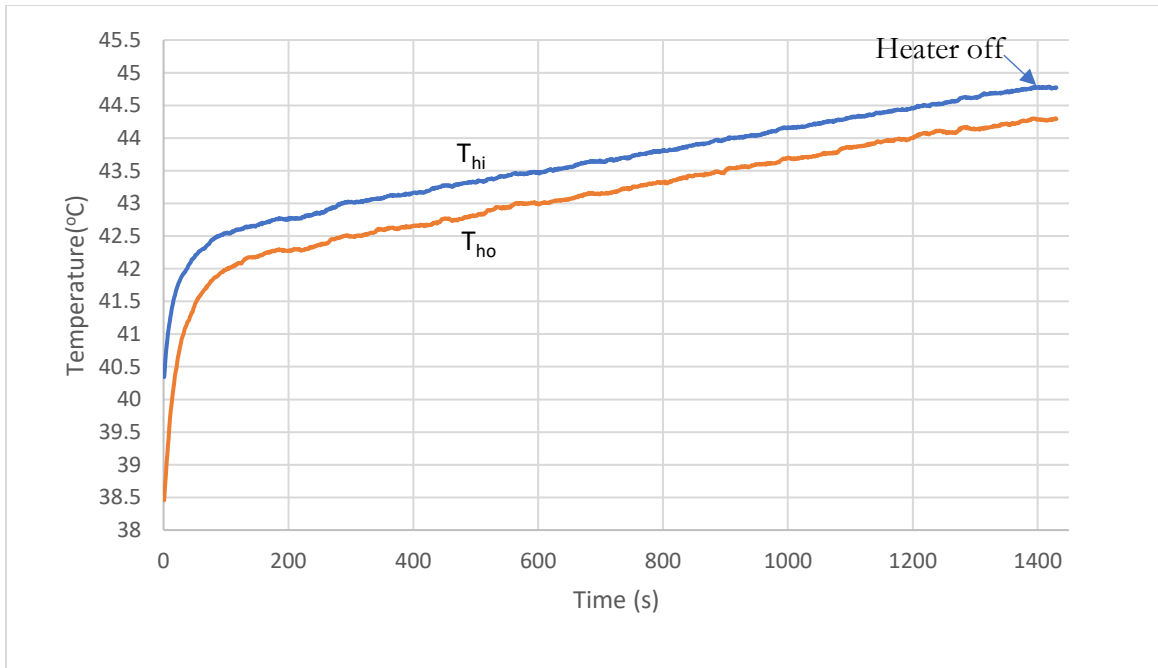


Fig. 23: Transient state response on the hot side for trial 2.

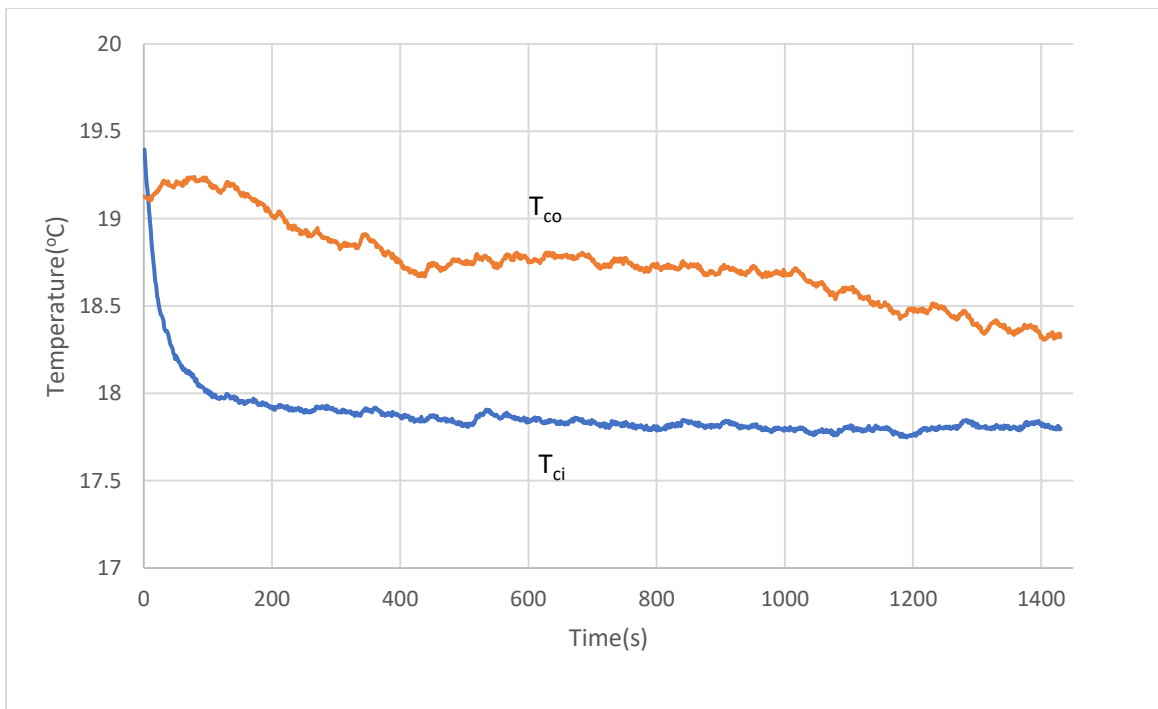


Fig. 24: Transient state response on the cold side for trial 2.

3.2 Heat Transfer Rate

Now comparing heat transferred on the hot side, the cold side and the maximum possible heat transfer rate, we get the following result shown in Table 4. Note that the flow rate of the cold side is fixed at 0.8 gpm ($5.05 \times 10^{-5} \text{ m}^3 \text{ s}^{-1}$). So, the minimum heat capacity rate C_{min} is always based on the cold side.

Table 4: Different heat transfer rates calculated from the data

Trial	\dot{Q}_{hot} (W)	\dot{Q}_{cold} (W)	\dot{Q}_{max} (W)	ε $= \frac{\dot{Q}_{hot}}{\dot{Q}_{max}}$	UA (WK ⁻¹)	C_{min} (WK ⁻¹)	C_{max} (WK ⁻¹)	NTU $= \frac{UA}{C_{min}}$	$\frac{C_{min}}{C_{max}}$
1	73.94	44.36	5160.85	0.0143	3.06	211.25	211.25	0.0145	1
2	103.51	109.85	5695.32	0.0182	3.91	211.25	211.25	0.0185	1
3	107.74	680.23	7345.18	0.0147	3.27	211.25	316.88	0.0155	0.67
4	120.41	640.09	5779.82	0.0208	4.70	211.25	316.88	0.0222	0.67
5	129.92	621.08	6229.78	0.0209	4.67	211.25	316.88	0.0221	0.67
6	101.40	173.22	6814.94	0.0149	3.20	211.25	422.5	0.0151	0.5
7	71.83	166.89	5129.16	0.0140	3.02	211.25	422.5	0.0143	0.5

We can observe that the heat transfer on the cold side is generally extremely high compared to the rate of heat loss on the hot side which has a relatively consistent heat transfer rate. So, the hot side heat transfer rate, \dot{Q}_{hot} , is used to evaluate the Number of Transfer Units (NTU). Since the temperature differences are within the uncertainty limits, the data obtained cannot be completely trusted. This could be due to a lack of sufficient time for the heat exchanger to attain steady-state conditions. This could also be due to the core heating up

and not having enough time to release the heat reflected in the cold side abnormalities. The material nylon – 12 sometimes retains water and the retained water at a relatively higher temperature could have sparked an anomaly in the cold side heat transfer.

3. 3. ε v NTU relationship

The data from the hot side is used in the effectiveness equation(11) and we can find a value for ε , and the NTU value for different values of $C_r = \frac{C_{min}}{C_{max}}$. Since the data points are not sufficient for a decent plot, we can use a logarithmic trendline to extrapolate using MATLAB to obtain the following plot shown in Fig 25. The data points used are marked in the figure.

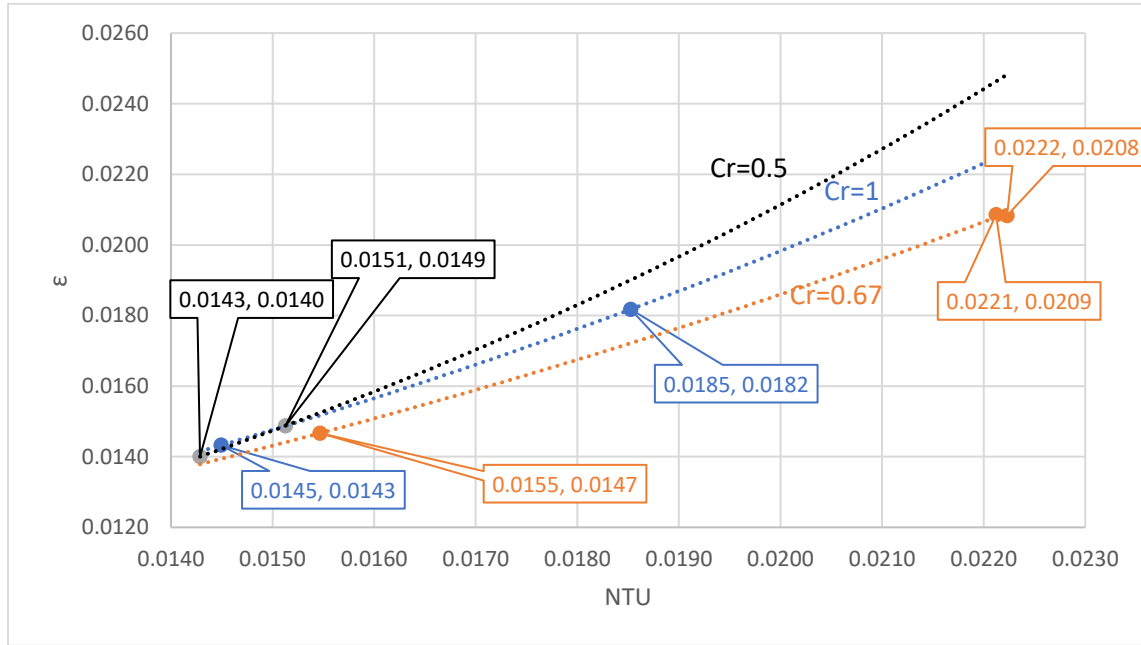


Fig 25: ε v NTU data for different capacity ratios.

The logarithmic functions for each capacity ratio are given below:

$$C_r = 1, \varepsilon = 0.0164 e^{0.1682NTU} \quad (13)$$

$$C_r = 0.67, \varepsilon = 0.01854e^{0.2025NTU} \quad (14)$$

$$C_r = 0.5, \varepsilon = 0.01443e^{0.0429NTU} \quad (15)$$

The NTU values calculated for similar effectiveness values for a counter-flow shell-and-tube heat exchanger is discussed in section 3.5

3.4. Pressure drop

Heat exchanger characterization is not complete without discussing the pressure loss across the heat exchanger. In this experiment, we use two U tube manometers and measure differential pressures based on the difference in heights of the two water columns. The flow rate of the cold side is fixed at 0.8 gpm ($5.05 \times 10^{-5} \text{ m}^3 \text{ s}^{-1}$) and because of the symmetry of the heat exchanger, the pressure difference is only measured on the hot side for flow rates between 0.8 gpm and 2.0 gpm. The differences in heights are tabulated in Table 5.

Table 5: Pressure measurements for the hot side of the heat exchanger

$\dot{V} \text{ (gpm)}$	$\Delta H \text{ (in)}$	$\Delta P \text{ (psi)}$	$\Delta P \text{ (Pa)}$
0.8	1.625	0.059	406.79
1.2	2.625	0.095	655.00
1.6	3.500	0.126	868.74
2.0	4.125	0.149	1027.32

The plot in Fig. 26 shows the relationship between flow rate and the pressure loss. The best-fit curve for the data obtained in the experiment is determined as

$$\Delta P = 0.0261\dot{V}^2 + 0.0508 \quad \text{RMS } 0.0106 \quad (16)$$

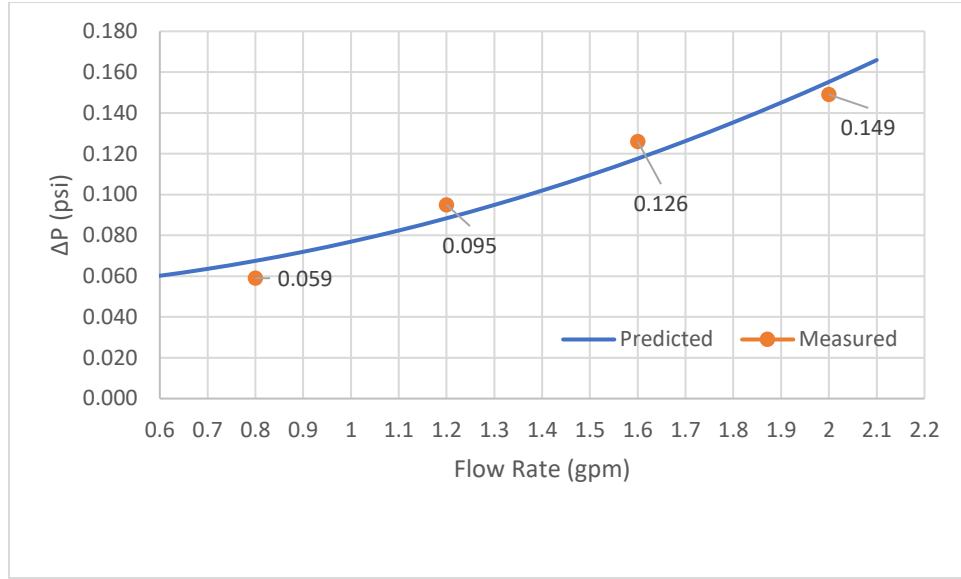


Fig 26: Pressure loss v flow rate in the Schwarz D heat exchanger.

The pressure loss in a pipe flow is directly related to the square of the average velocity, $\Delta P \propto V^2$. The average velocity is proportional to the flow rate. So, we can plot a polynomial curve of order 2 as the best-fit curve.

3.5 Comparison to conventional heat exchangers

We can compare our results to a conventional heat exchanger in terms of material used, effective pressure loss and performance. For this comparison we need to determine the hydraulic diameter of the flow. For the Schwarz D geometry, we can find the average area of the cross section of the fluid flow by inspecting a thin cross section. The average channel cross-sectional area is determined to be 193.69 mm^2 . From this the hydraulic diameter, D_H , is found to be 15.72 mm . The total volume, V_t , occupied by the Schwarz D core is 1157.625 cm^3 (cube of side 10.5 cm). The volume of material, V_m , used for printing the heat exchanger is 339.2 cm^3 . The fluid volume, V_f , is the difference between the two: $V_f = 818.425 \text{ cm}^3$.

The total effective length of straight pipe L_{eff} is found from

$$V_f = \frac{2\pi \cdot D_H^2 \cdot L_{eff}}{4} \quad (17)$$

and is found to be 210.84 cm. The heat transfer surface area A , calculated using L_{eff} and D_H , is 1040.72 cm². For the same heat transfer surface area and hydraulic diameter, a shell-and-tube heat exchanger core of same length will occupy a volume of 1524.53 cm³ (densely packed 20 cylinders of length 10.5 cm and 2 mm thick walls). Compared with the shell-and-tube heat exchanger, the Schwarz D model is more compact and occupies 32% less space.

The Schwarz D geometry is equivalent to 20 tubes of length 10.5 cm with the same hydraulic diameter, D_H . We can compare the friction factor for the Schwarz D geometry, f_D for different flow rates using the pipe flow friction factor equation:

$$f_D = \frac{\Delta P \pi^2 D_H^5}{32 \dot{V}^2 L \rho} \quad (18)$$

The Reynolds number for the flow in the tube were found to be within the laminar region.

The friction factor for the pipe in shell-and-tube heat exchanger, f_p can be evaluated as [9]:

$$f_p = 64/R_e \quad (18)$$

We can use this to evaluate a correlation factor ω for the Schwarz D geometry for laminar flow, where,

$$f_D = \omega \frac{64}{R_e} \quad (19)$$

The friction factors can be found in Table 7.

Table 7: Friction factors for Schwarz D geometry and shell-and-tube:

\dot{V} (gpm)	Re	f_D	f_p	$\omega = \frac{f_D}{f_p}$
0.8	229.96	178.57	0.28	637.75
1.2	344.94	127.36	0.19	670.32
1.6	459.92	95.01	0.14	678.64
2.0	574.9	71.91	0.11	653.73

Compared to the flow in a pipe, the Schwarz D geometry has a higher frictional loss if the laminar flow case is considered. In the Schwarz D heat exchanger, geometry is a major cause of flow disturbances due to internal mixing within the hot and cold fluid channels. Assuming the laminar flow condition in an equivalent pipe does not consider the loss due to friction, hence the correlation factor ω is significantly higher but are on the same order of magnitude. The variation friction factors for Schwarz D (f_D) and the pipe (f_p) compared with the estimated friction factor from Fanning's results ($f_t = \frac{233}{Re}$) are shown in Fig. 27.

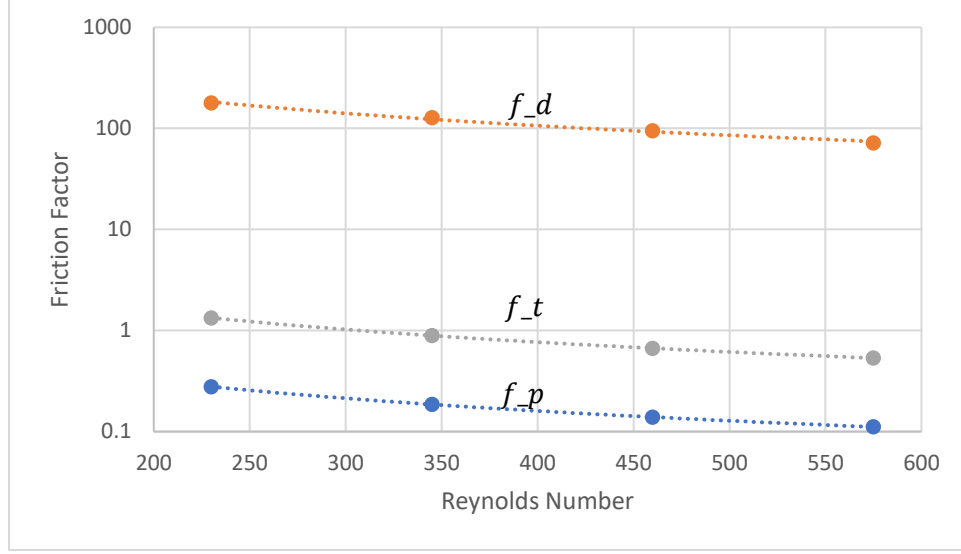


Fig 27: Friction factor v Reynolds number

3.6 Estimating overall heat transfer coefficient, U

The overall heat transfer coefficient, U can be calculated by using the equation

$$U = \left(\frac{1}{h} + \frac{t}{k_n} + \frac{1}{h} \right)^{-1} \quad (20)$$

where h is the convective heat transfer coefficient, t the wall thickness and k_n the thermal conductivity of nylon [9].

The convective heat transfer coefficient can be estimated using the Nusselt number, N_u ,

$$N_u = \frac{hL}{k_w} \quad (21)$$

where h is the convective heat transfer coefficient, D_H the hydraulic diameter and k_w the thermal conductivity of water [9].

For a Schwarz D geometry, the Nusselt number can be calculated using the equation,

$$N_u = aR_e^b P_r^{1/3} \quad (22)$$

where R_e is the Reynolds number, P_r the Prandtl number, a (1.20) and b (1.81) are characteristic parameters for the Schwarz D geometry [9].

The overall heat transfer coefficient using this method was found to be $36.1 \text{ W K}^{-1}\text{m}^{-2}$.

3.7 Discussions

The results obtained in the study were within the uncertainty limits. This can be improved with some updates to both the heat exchanger and the experiment.

The heat exchanger wall thickness was 4 mm which can be reduced by manipulating the thickness of the Schwarz D geometry in Mathematica. A custom python program can be written to easily control the thickness of the geometry, which significantly improves the heat transferred. The current design of the heat exchanger manifolds can have null spaces in the heat exchanger where the flow is stagnated or there is no fluid flow. Increasing the number of inlet ports can provide an evenly distributed flow pattern inside the heat exchanger. Cross flow design provides the best flow distribution, where a single inlet can be distributed to all available flow channels. Transparent resin-based material can be used to print the heat exchanger for a better visual understanding of the flow. Nylon has a low thermal conductivity, thermally conductive plastics or metal embedded plastics or even metals can be used to print the heat exchanger for better results from the experiment.

Some changes in the experiment design can improve the results. The manifold can be integrated into the fluid line instead of the pipes connecting into the heat exchanger for higher operational pressures. A closed-loop temperature control drastically improves the steady state performance, avoiding the high uncertainties in the current design by keeping the inlet temperatures at a fixed level. Instrumentation upgrades can lower the uncertainties in the results. The thermocouples must be mounted closer to the flow to avoid errors in measurements due to eddies.

CHAPTER 4

CONCLUSION

The primary goal of this study was to try and break free from the established design norms and explore new possibilities, taking advantage of the latest technologies like 3D printing in thermal applications. As a first phase of this research, this study was conducted to establish an understanding of the behavior of heat exchangers with complex 3D geometries. The study explored several ways of generating TPMS geometries, applying different 3D printing technologies like FDM and SLS to build prototype heat exchangers.

The experimental results show some abnormalities in the cold side for the temperatures and the heat transfer rates. The hot side has a consistent difference across all trials. But the data acquired are within the uncertainty limits, so no definitive conclusions can be drawn from the data. There are several anomalies expected due to internal mixing and the geometrical factors in this case. The steady-state from the hot side was used to determine the effectiveness of the heat exchanger and the NTU- ϵ relation which were also within uncertainty limits.

For same heat transfer surface area and hydraulic diameter, the volume occupied by a shell-and-tube heat exchanger can be calculated. Compared to the shell-and-tube geometry, the Schwarz D geometry occupies less volume and is smaller by 32%. The friction factor for the shell-and-tube heat exchanger and the Schwarz D geometry followed similar trends, as observed in the studies by Femmer[9], with increasing Reynolds number.

CHAPTER 5

FUTURE WORK

Being a relatively new area of research, a more comprehensive study should be conducted with extensive experiments and in a more controlled environment. This would allow us to refine the effectiveness relationships obtained by extrapolation.

Computational study needs to be done to better understand the flow paths inside the complex geometry to help optimize the shape of the heat exchanger for better performance.

New materials like carbon/copper embedded plastics that have higher conductivity than nylon – 12 can be used to fabricate the heat exchangers, bridging the gap between metal and polymer heat exchangers.

REFERENCES

- [1] Meeks III, William H., and Joaquín Pérez. "The Classical Theory Of Minimal Surfaces". *Bulletin Of The American Mathematical Society*, vol 48, no. 3, 2011, pp. 325-325. American Mathematical Society (AMS), doi:10.1090/s0273-0979-2011-01334-9. Accessed 23 Mar 2018.
- [2] NASA Electronics Research Center; Cambridge, MA, United States. *Infinite Periodic Minimal Surfaces Without Self-Intersections*. 1970. Accessed 23 Mar 2018
- [3] van der Net, A. (n.d.). *Plateau's Memory*. [Metal].
- [4] Zeleny, Enrique. "Wolfram Demonstrations Project". Wolfram Demonstrations Project, 2013, <http://demonstrations.wolfram.com/TriplyPeriodicMinimalSurfaces/>. Accessed 23 Mar 2018.
- [5] Baumer, Martin et al. *The Economics Of 3D Printing: A Total Cost Perspective*. Oxford, https://www.sbs.ox.ac.uk/sites/default/files/research-projects/3DP-RDM_report.pdf. Accessed 26 Mar 2018.
- [6] "FORMIGA P 110 - Laser Sintering 3D Printer – EOS". Eos.Info, 2018, https://www.eos.info/systems_solutions/plastic/systems_equipment/formiga_p_110. Accessed 23 Mar 2018.
- [7] Chen, Xiangjie et al. "Recent Research Developments In Polymer Heat Exchangers – A Review". *Renewable And Sustainable Energy Reviews*, vol 60, 2016, pp. 1367-1386. Elsevier BV, doi:10.1016/j.rser.2016.03.024.
- [8] Arie, Martinus A. et al. "Experimental Characterization Of Heat Transfer In An Additively Manufactured Polymer Heat Exchanger". *Applied Thermal Engineering*, vol 113, 2017, pp. 575-584. Elsevier BV, doi:10.1016/j.applthermaleng.2016.11.030.
- [9] Femmer, Tim et al. "Estimation Of The Structure Dependent Performance Of 3-D Rapid Prototyped Membranes". *Chemical Engineering Journal*, vol 273, 2015, pp. 438-445. Elsevier BV, doi:10.1016/j.cej.2015.03.029.
- [10] PA2200 Product Information. EOS Gmbh - Electro Optical Systems, 2010, p. 1, Accessed 23 Mar 2018.
- [11] Çengel, Yunus A. *Heat And Mass Transfer*. Mcgraw-Hill, 2007.

[12]Moffat, R. J. "Using Uncertainty Analysis In The Planning Of An Experiment". Journal Of Fluids Engineering, vol 107, no. 2, 1985, p. 173. ASME International, doi:10.1115/1.3242452.

APPENDIX A
MATHEMATICA CODE

Creates a 3D geometry Plot

```
Manipulate[  
  geometry=
```

```
ContourPlot3D[Sin[x]Sin[y]Sin[z]+Cos[x]Sin[y]Cos[z]+Cos[y]Sin[z]Cos[x]+Cos[z]Sin[x]Cos[  
y]=0,{x,-r,r},{y,-r,r},{z,-r,r},Axes->False,Mesh->False,Background->Black,Boxed-  
>False,MaxRecursion->mr,Contours->1,MeshFunctions->Automatic,BoundaryStyle-  
>If[style=="color",Directive[Yellow,Thick,Opacity[op]],None],RegionFunction-  
>Function[{x,y,z},If[region=="cube",(True),Norm[{x,y,z}]<r]],ContourStyle-  
>If[style=="color",{Opacity[op],Specularity[White,30],FaceForm[Orange,Blue]},{Opacity[o  
p],Specularity[White,10],Lighting-  
>"Neutral",Texture[ExampleData[{"Texture","Straw"}]]}],PerformanceGoal:>"Speed",Ima  
geSize->400,SphericalRegion->True,PlotTheme->"ThickSurface"],
```

```
{ {r,10,"range"},1,10,ImageSize->Tiny},  
{ {op,6,"opacity"},1,3,ImageSize->Tiny},  
{ {mr,1,"recursion"},{0,1,2,3}},  
{style,{"color","texture"}},  
{region,{"cube"}},ControlPlacement->Left]
```

Creates discretized points

```
geometry2 = DiscretizeGraphics[geometry]
```

Creates a Mesh

```
geometry3 = MeshRegion[geometry2, PlotTheme -> "Lines"]
```

Saves mesh as a STL file

```
Export["S_D1.stl", geometry3]
```

APPENDIX B

STEADY-STATE TEMPERATURE DATA

TRIAL 1

Time	T_hi	T_ci	T_ho	T_co
1	32.59852	8.151139	32.25498	8.336994
2	32.60859	8.147521	32.25132	8.345938
3	32.59671	8.137849	32.24394	8.351676
4	32.59986	8.14686	32.25993	8.352861
5	32.59791	8.160687	32.24964	8.359573
6	32.58114	8.145863	32.23984	8.348073
7	32.59214	8.157456	32.24004	8.349944
8	32.58755	8.147872	32.24084	8.346764
9	32.5825	8.150618	32.23129	8.34619
10	32.57205	8.139374	32.22759	8.343246
11	32.59257	8.156484	32.22988	8.348024
12	32.57651	8.145016	32.22417	8.352441
13	32.57945	8.143131	32.23229	8.350794
14	32.58641	8.155212	32.23566	8.363817
15	32.58359	8.152006	32.23103	8.342126
16	32.57303	8.156524	32.23983	8.356359
17	32.57588	8.153366	32.23165	8.360787
18	32.58506	8.1628	32.23858	8.357419
19	32.5801	8.154489	32.22371	8.360014
20	32.58022	8.159357	32.21775	8.358481
21	32.57918	8.153042	32.21648	8.356435
22	32.572	8.158521	32.22213	8.354327
23	32.57327	8.1563	32.21507	8.35424
24	32.57277	8.157911	32.21232	8.362485
25	32.56424	8.154853	32.21144	8.359904
26	32.56209	8.166097	32.21919	8.364033
27	32.57015	8.165348	32.22028	8.366839
28	32.56216	8.169966	32.21363	8.371218
29	32.5697	8.168906	32.22501	8.368262
30	32.56723	8.167247	32.20925	8.359968
31	32.56788	8.168644	32.20945	8.377243
32	32.55172	8.171777	32.2131	8.379189
33	32.55969	8.178278	32.21613	8.395641
34	32.56247	8.180487	32.21687	8.399982
35	32.55643	8.183607	32.22862	8.403337
36	32.54707	8.175883	32.2143	8.404622
37	32.54727	8.184394	32.2109	8.419763

TRAIL 2

Time	T_hi	T_ci	T_ho	T_co
1	44.77389	17.82499	44.28988	18.32014
2	44.77066	17.82483	44.28027	18.32392
3	44.78032	17.81136	44.28137	18.32507
4	44.77714	17.82866	44.28587	18.318
5	44.76586	17.81302	44.28228	18.30795
6	44.77308	17.81787	44.28138	18.31256
7	44.77412	17.81502	44.28483	18.3074
8	44.76506	17.80613	44.27796	18.30849
9	44.77632	17.81897	44.28505	18.31366
10	44.78249	17.8104	44.27958	18.31508
11	44.76571	17.80776	44.27136	18.31452
12	44.77366	17.80989	44.27778	18.32384
13	44.77605	17.82054	44.27907	18.33749
14	44.77051	17.8126	44.27638	18.3328
15	44.77109	17.80439	44.2662	18.32994
16	44.77812	17.80532	44.2662	18.33643
17	44.76749	17.79919	44.26985	18.32869
18	44.78243	17.80848	44.26809	18.34261
19	44.77652	17.80618	44.27361	18.34936
20	44.78765	17.79891	44.27947	18.34626
21	44.77496	17.79873	44.28259	18.3317
22	44.78312	17.79552	44.2756	18.3118
23	44.76272	17.80088	44.27716	18.32759
24	44.76401	17.80341	44.29142	18.33313
25	44.75704	17.79301	44.27169	18.32785
26	44.7667	17.79603	44.27982	18.31881
27	44.76669	17.80554	44.28948	18.33758
28	44.76913	17.81369	44.29104	18.33714
29	44.76991	17.80964	44.29842	18.33588
30	44.76272	17.79298	44.28683	18.32342
31	44.77589	17.80111	44.30177	18.34127
32	44.7715	17.79484	44.29144	18.32272

TRIAL 3

Time	T_hi	T_ci	T_ho	T_co
1	40.18627	5.357002	39.8482	8.597448
2	40.17095	5.344331	39.84862	8.593396
3	40.17496	5.351502	39.84087	8.584881
4	40.17619	5.357128	39.84543	8.592126
5	40.16623	5.360722	39.8348	8.613932
6	40.16528	5.371623	39.83984	8.604147
7	40.17366	5.373732	39.83448	8.597951
8	40.18444	5.389389	39.84814	8.614444
9	40.1719	5.385434	39.84048	8.622361
10	40.17975	5.392693	39.84545	8.614171
11	40.16955	5.395543	39.83324	8.602315
12	40.17719	5.381581	39.83778	8.611192
13	40.17683	5.395982	39.8301	8.611042
14	40.16749	5.394048	39.83141	8.61907
15	40.17242	5.3972	39.83811	8.612962
16	40.16459	5.406192	39.8376	8.621889
17	40.17578	5.406781	39.83681	8.628869
18	40.15513	5.406266	39.82148	8.611304
19	40.16811	5.398532	39.81495	8.618548
20	40.14537	5.389078	39.81636	8.608924
21	40.15168	5.403027	39.80804	8.605009
22	40.13915	5.399083	39.80415	8.611752
23	40.14682	5.407336	39.81338	8.608339
24	40.13785	5.393624	39.80751	8.60491
25	40.1397	5.39085	39.79916	8.608077
26	40.13789	5.398207	39.80977	8.606855
27	40.13935	5.40097	39.80014	8.621206
28	40.13843	5.399978	39.79656	8.605772
29	40.13632	5.392697	39.79289	8.602095
30	40.13434	5.395334	39.79401	8.611108
31	40.1238	5.40165	39.79589	8.606721
32	40.13203	5.403824	39.80346	8.624513
33	40.12862	5.401825	39.81158	8.614475

TRIAL 4

Time	T_hi	T_ci	T_ho	T_co
1	30.54547	3.18222	30.16437	6.21197
2	30.58149	3.179777	30.18653	6.199272
3	30.58753	3.19266	30.19937	6.213974
4	30.57847	3.185921	30.18713	6.2149
5	30.59223	3.203636	30.19977	6.232734
6	30.57025	3.194701	30.17709	6.208857
7	30.57746	3.191091	30.18545	6.215511
8	30.5804	3.19205	30.18545	6.209082
9	30.57561	3.183128	30.18087	6.219746
10	30.5721	3.192829	30.17578	6.222476
11	30.55634	3.185699	30.17244	6.213727
12	30.57318	3.193017	30.17573	6.222187
13	30.55353	3.186556	30.16285	6.210768
14	30.54946	3.176964	30.15561	6.198384
15	30.54622	3.180005	30.15169	6.207595
16	30.5433	3.174982	30.1612	6.196414
17	30.52994	3.171599	30.14399	6.193292
18	30.52407	3.178804	30.15011	6.197591
19	30.53195	3.172531	30.15844	6.199219
20	30.53123	3.175849	30.15433	6.200371
21	30.53738	3.187646	30.16433	6.207803
22	30.53749	3.191115	30.16353	6.205295
23	30.52634	3.187922	30.15283	6.203791
24	30.53076	3.179428	30.15499	6.213213
25	30.52591	3.189144	30.15918	6.222864
26	30.51991	3.177508	30.14617	6.208926
27	30.51689	3.175502	30.14903	6.217886
28	30.52503	3.175021	30.15762	6.222886
29	30.52052	3.171916	30.15333	6.221469
30	30.50026	3.165049	30.14753	6.223221
31	30.50534	3.164922	30.14289	6.226429
32	30.50917	3.171863	30.14039	6.221178

TRIAL 5

Time	T_hi	T_ci	T_ho	T_co
1	33.05024	3.587241	32.63861	6.535234
2	33.0484	3.589597	32.64038	6.538288
3	33.05762	3.596064	32.64218	6.543523
4	33.04906	3.59628	32.64103	6.529222
5	33.0485	3.59904	32.64385	6.540768
6	33.05361	3.594186	32.64491	6.53666
7	33.05162	3.587277	32.6517	6.525514
8	33.07022	3.587933	32.66086	6.543536
9	33.05407	3.591324	32.6636	6.543573
10	33.06082	3.578389	32.65347	6.525964
11	33.06971	3.586432	32.6554	6.529195
12	33.06426	3.588047	32.663	6.538652
13	33.08026	3.59072	32.66866	6.529409
14	33.06515	3.582764	32.67739	6.52103
15	33.06647	3.581302	32.67624	6.538852
16	33.08117	3.575161	32.67767	6.524185
17	33.07754	3.579195	32.67921	6.527955
18	33.07552	3.575854	32.68304	6.529395
19	33.0594	3.566336	32.6759	6.508517
20	33.07634	3.567623	32.67756	6.51979
21	33.08438	3.575464	32.67188	6.498785
22	33.08145	3.559894	32.67953	6.518775
23	33.0862	3.571657	32.6782	6.508091
24	33.08447	3.560233	32.67715	6.501502
25	33.08963	3.566928	32.68636	6.504345
26	33.08235	3.550791	32.67165	6.489504
27	33.09382	3.552947	32.67345	6.493074
28	33.08771	3.544525	32.67837	6.49494
29	33.08868	3.548194	32.67124	6.481688

Trial 6

Time	T_hi	T_ci	T_ho	T_co
1	39.96715	7.673753	39.68262	8.496401
2	39.96991	7.66697	39.69802	8.496739
3	39.96902	7.678365	39.70312	8.490107
4	39.95392	7.670984	39.69512	8.489136
5	39.96496	7.680191	39.70838	8.503301
6	39.96438	7.690725	39.7078	8.510736
7	39.96114	7.686776	39.70744	8.503478
8	39.96211	7.682594	39.70974	8.495275
9	39.96637	7.683833	39.71001	8.49983
10	39.9571	7.672963	39.70872	8.503905
11	39.96352	7.679361	39.7147	8.509107
12	39.94316	7.675364	39.695	8.484979
13	39.94171	7.666221	39.70264	8.490541
14	39.94271	7.677727	39.70319	8.484257
15	39.95766	7.68234	39.70063	8.492416
16	39.94519	7.666147	39.69903	8.487862
17	39.93633	7.681105	39.69482	8.494974
18	39.92162	7.676045	39.69297	8.489449
19	39.94746	7.670712	39.69863	8.484125
20	39.92804	7.670338	39.6812	8.480909
21	39.93057	7.680635	39.69127	8.48716
22	39.94256	7.680185	39.68442	8.513483
23	39.93264	7.676203	39.69423	8.507139
24	39.9315	7.683773	39.686	8.502612
25	39.93559	7.686959	39.6974	8.495605
26	39.93278	7.689883	39.69636	8.513687
27	39.92401	7.689759	39.69048	8.508351
28	39.92338	7.700478	39.68431	8.506256
29	39.91913	7.697819	39.68271	8.506919
30	39.90693	7.699717	39.69003	8.502418
31	39.92043	7.698982	39.69755	8.510687
32	39.92242	7.700362	39.69022	8.499776

TRIAL 7

Time	T_hi	T_ci	T_ho	T_co
1	30.84702	6.520961	30.67466	7.324335
2	30.84002	6.525006	30.6654	7.329323
3	30.84141	6.518142	30.66747	7.324609
4	30.83477	6.531368	30.66263	7.324509
5	30.85193	6.527323	30.67438	7.334249
6	30.85417	6.547524	30.67977	7.351563
7	30.84044	6.525682	30.6744	7.330235
8	30.84177	6.527084	30.6798	7.344462
9	30.84178	6.536139	30.66444	7.337111
10	30.84305	6.524867	30.6743	7.343674
11	30.84426	6.53138	30.66874	7.334735
12	30.84336	6.544705	30.66806	7.342098
13	30.84719	6.541362	30.67731	7.3504
14	30.83966	6.541524	30.67023	7.348899
15	30.8474	6.549439	30.67662	7.355137
16	30.8399	6.561048	30.6829	7.369101
17	30.8395	6.554436	30.69018	7.357988
18	30.83412	6.561385	30.68209	7.368963
19	30.83475	6.556101	30.67278	7.360362
20	30.84073	6.566206	30.68147	7.365224
21	30.83713	6.552895	30.66183	7.352174
22	30.83411	6.558993	30.67349	7.366337
23	30.83455	6.558266	30.67325	7.353023
24	30.82421	6.54856	30.66223	7.347134
25	30.82477	6.541772	30.66234	7.340121
26	30.827	6.548409	30.65779	7.339858
27	30.82343	6.5437	30.64609	7.330881
28	30.82845	6.559693	30.65699	7.337583
29	30.82361	6.552216	30.6413	7.328218
30	30.82482	6.547069	30.64229	7.340895
31	30.81415	6.551051	30.6307	7.315653
32	30.81983	6.559893	30.63187	7.319966